THE DESIGN AND FLOW SIMULATION OF A POWER-AUGMENTED SHROUD FOR URBAN WIND TURBINE SYSTEM

WONG KOK HOE

INSTITUTE OF GRADUATE STUDIES
UNIVERSITY OF MALAYA
KUALA LUMPUR

2013

THE DESIGN AND FLOW SIMULATION OF A POWER-AUGMENTED SHROUD FOR URBAN WIND TURBINE SYSTEM

WONG KOK HOE

SUBMITTED TO THE FACULTY OF ENGINEERING UNIVERSITY OF MALAYA, IN PARTIAL FULFILMENT OF THE REQUIREMENT FOR THE DEGREE OF MASTER OF MECHANICAL ENGINEERING

2013

UNIVERSITI MALAYA

ORIGINAL LITERARY WORK DECLARATION

Name of Candidate: Wong Kok Hoe

Registration/Matric No: KGY110005

Name of Degree: Master of Mechanical Engineering

Title of Project Paper/Research Report/Dissertation/Thesis ("this Work"):

THE DESIGN AND FLOW SIMULATION OF A POWER-AUGMENTED SHROUD FOR URBAN WIND TURBINE SYSTEM

Field of Study:

I do solemnly and sincerely declare that:

(1) I am the sole author/writer of this Work;
(2) This Work is original;
(3) Any use of any work in which copyright exists was done by way of fair dealing and for permitted purposes and any excerpt or extract from, or reference to or reproduction of any copyright work has been disclosed expressly and sufficiently and the title of the Work and its authorship have been acknowledged in this Work;
(4) I do not have any actual knowledge nor do I ought reasonably to know that the making of this work constitutes an infringement of any copyright work;
(5) I hereby assign all and every rights in the copyright to this Work to the University of Malaya ("UM"), who henceforth shall be owner of the copyright in this Work and that any reproduction or use in any form or by any means whatsoever is prohibited without the written consent of UM having been first had and obtained;
(6) I am fully aware that if in the course of making this Work I have infringed any copyright whether intentionally or otherwise, I may be subject to legal action or any other action as may be determined by UM.

Candidate's Signature Date

Subscribed and solemnly declared before,

Witness's Signature Date

Name:
Designation:

ABSTRACT

The depletion of fossil fuel and the increase of energy demand in the world make renewable energy become an alternative energy source. Among these green energies, the wind energy is one of the popular energy sources since decades ago. Recently, there are small wind turbine developments which are suitable for urban and suburban application. However, the efficiency of the wind turbine is the main concern for all researchers due to the uncertainty of wind speed and direction in urban area.

In this paper, a new power augmented shroud integrated with vertical axis wind turbine (VAWT) is introduced. This power augmented shroud is able to improve the performance of the VAWT significantly by increasing the wind speed, channel the flow to better angle of attack for the VAWT and reduce the negative torque of the wind turbine. Hence, it improves the self-starting of the VAWT, and increase the coefficient of power.

The numerical method is used to simulate the wind flow for the power augmented shroud with a single bladed NACA 0015 airfoil VAWT by commercial computational fluid dynamic (CFD) software ANSYS FLUENT 14.0. In this 2D simulation, the shear stress transport (SST) k-ω turbulence model with the sliding mesh method was used with the tip speed ratio of 5.1 for the wind turbine. The result is verified by re-simulate the experiment published by Sandia National Laboratories.

The simulation result shows that the new design of power augmented shroud is able the increase the coefficient of power significant for the VAWT which is about 115.56% compare to the bare VAWT. Therefore, for urban area application, this power augmented shroud can solve the low efficiency problem for the VAWT.

ABSTRAK

Susutan bahan api fosil dan peningkatan permintaan tenaga di dunia menyebabkan tenaga boleh diperbaharui menjadi sumber tenaga alternatif. Antara tenaga "hijau" ini, tenaga angin adalah salah satu sumber tenaga yang popular sejak beberapa dekad yang lalu. Baru-baru ini, terdapat pembangunan turbin angin kecil yang sesuai untuk kawasan bandar. Walau bagaimanapun, kecekapan turbin angin diberi keutamaan untuk semua penyelidik kerana ketidaktentuan kelajuan angin dan arah angin di kawasan bandar.

Dalam kajian ini, satu kafan baru yang disepadukan dengan VAWT (turbin angin paksi menegak) untuk menambah kuasa telah diperkenalkan. Kafan ini mampu meningkatkan prestasi VAWT dengan meningkatkan kelajuan angin dan menyalurkan pengaliran angin ke sudut yang lebih baik untuk VAWT. Ini dapat mengurangkan tork negatif turbin angin. Oleh itu, ia meningkatkan pemutaran mula VAWT, dan meningkatkan pekali kuasa.

Kaedah berangka telah digunakan untuk membuat simulasi aliran angin bagi kafan dengan VAWT berbilah tunggal (NACA 0015-airfoil). Perisian komersial CFD (Dinamik Bendalir Komputeran) ANSYS FLUENT 14.0 telah digunakan untuk simulasi ini. Dalam simulasi 2D ini, model gelora "Shear Stress Transport (SST) k-ω" dan kaedah "Sliding mesh" telah digunakan untuk simulasi turbin angin denagn nisbah kelajuan hujung 5.1. Hasilnya disahkan oleh simulasi semula eksperimen yang diterbitkan oleh "Sandia National Laboratories".

Hasil simulasi menunjukkan bahawa integrasi reka bentuk kafan baru dengan VAWT mampu meningkatan pekali kuasa bagi VAWT dengan ketara, iaitu kira-kira 115.56% berbanding dengan VAWT sahaja. Oleh itu, untuk kawasan bandar, kafan bertambah kuasa ini boleh menyelesaikan masalah kecekapan rendah untuk VAWT.

ACKNOWLEDGEMENT

First and foremost, the author would like to express the deepest appreciation to project supervisor, Dr. Chong Wen Tong, senior lecturer of Department of Mechanical Engineering, University of Malaya, who offer this research topic as the research project to fulfil the Master of Engineering programme. Besides, I would like to show my gratitude on the guidance and advice given along the project.

TABLE OF CONTENTS

LIST OF FIGURES

LIST OF TABLES

LIST OF SYMBOLS AND ABBREVIATION

AOA	Angle of attack, rad
α	Wake factor
A	Area, cross section, m^2
c	Blade chord, m
CFD	Computational fluid dynamics
Cp	Coefficient of power
Cp, max	Maximun value of power coefficient
Ct	Tangential force coefficient
Cn	Normal force coefficient
D	Drag force, N
d	Displacement height, m
$D\omega$	Cross-diffusion term
DNS	Direct Numerical Simulation
DES	Detached Eddy Simulation
F	Force, N
Fr	Resultant force, N
Ft	Tangential force, N
Fn	Normal force, N
$\vec{F}$	External body forces, N
$Ft\ avg$	Average tangential force, N
$Fn\ avg$	Average normal force, N
FDM	Finite difference method

FEM	Finite element method
FVM	Finite volume method
$\tilde{G}k$	Generation of turbulence kinetic energy due to mean velocity gradient
$G\omega$	Generation of ω
H	Height of the turbine, H
HAWT	Horizontal axis wind turbine
I	Unit tensor
IGEM	International Greentech and Eco Products Exhibition and Conference Malaysia
k	Von Karman's constant
L	Lift force, N
LES	Large Eddy Simulation
$\dot{m}$	Mass flow rate, kg/s
N	Number of blade for VAWT
ODGV	Omni-Directional Guide Vane
P	Power, W
ρ	Density, kg/m^3
p	Static pressure, Pa
$\rho.\vec{g}$	Gravitational body force, N
PAGV	Power augment guide vane
R	Rotor radius, m
RANS	Reynolds-Averaged Navier-Strokes
RSM	Reynolds Stress Model
Sm	Source term

SA	Spalart-Allmaras
SST	The Shear- stress transport
Sk , $S\omega$	User defined source terms
SIMPLE	Semi-Implicit Method for Pressure Linked Equations
T	Torque generated, Nm
$\bar{\bar{T}}$	Stress tensor
Γk	Effective diffusivity of k
$\Gamma\omega$	Effective diffusivity of ω
τw	Wall shear stress
TNB	Tenaga National Berhad
TSR	Tip speed ratio
U	Tip speed, m/s
μ	Molecular viscosity, kg/ms
u*	Friction velocity, m/s
$\bar{u}(z)$	Average wind speed at height z above ground, m
Uh	Wind speed at height h, m
v	Wind stream velocity, m/s
vo	Undisturbed wind speed, m/s
Vc	Chordal velocity component, m/s
Vn	Normal velocity component, m/s
Va	Iinduced flow velocity, m/s
VAWT	VAWT ertical axis wind turbine
VGOT	Variable geometry oval trajectory
ω	Angular velocity, rad/s

W	Local relative flow velocity, m/s
Yk	Dissipation of k
$Y\omega$	Dissipation of ω
y	Distance from the wall to the cell center, m
zo	Roughness length, m
θ	Azimuth angle, rad

LIST OF APPENDICES

CHAPTER 1 INTRODUCTION

1.1 Introduction

According to The United Nations Environment Programme "21 Issues for the 21st Century", creating clean renewable energy is ranked as second among the top ten environmental problems which human being face in future. As the demand of energy is increasing, human race are challenged to change the use of fossil fuel to a "clean" renewable energy, (http://www.safety-security-crazy.com/major-environmental-issues.html, 9/10/2012).

For Malaysia, data from Tenaga National Berhad (TNB) show that the electricity generating capacity increased by 20% between year 2000 till 2009. It shows a great increase of demand in a decade. Currently TNB reserve margin of 31%, but it is predicted that the margin will drop to 20% by year 2015, if no new power plant is setup. As countermeasure for this energy demand, Malaysia aim for 5.5% renewable energy share in installed capacity by 2015, where the government target to achieve 40% cut in carbon emissions by 2020 according to the prime minister Dato' Sri Najib Razak during the International Greentech and Eco Products Exhibition and Conference Malaysia (IGEM 2012). This shows the high concern and determination of Malaysia government on the energy saving goals (http://www.renewableenergyworld.com/rea/news/article/2011/09/malaysia-explores-its-renewables-options, 15/10/12).

Wind energy has been used in agriculture sector since hundreds years ago for water pumping. This clean technology developed rapidly, and it is one of the preference candidates for the aim of increase the energy share of renewable energy.

1.2 Wind turbine

Generally there are two types of wind turbine which are horizontal axis wind turbine (HAWT) and vertical axis wind turbine (VAWT). HAWT has been use since century ago. Comparing both wind turbines, the ideal efficiency for VAWT is more than 70%, whereas the ideal efficiency for HAWT is about 50-60%. There are several advantages of VAWT compare to HAWT. Among these advantages, the first is the construction of VAWT is much simpler than HAWT. VAWT is omni-direction to the incoming wind; therefore it does not need yaw mechanism to detect the wind direction where HAWT is highly depending on this yaw mechanism. Due to the omni-direction incoming wind, the VAWT have small sway space and footprint for the installation, where the blade's operation space is small. Besides, less noise produce and visual impact, less obstruction to birds and the low installation height from ground, make this wind turbine become popular in urban area. However, the main drawback for the VAWT compare to HAWT is low efficiency in self-starting mechanism (Aslam Bhutta et al., 2012; Eriksson, Bernhoff, & Leijon, 2008; Mohamed, 2012; Toja-Silva, Colmenar-Santos, & Castro-Gil, 2013).

In Malaysia, the wind speed is low throughout the year. Every wind turbine needs to have certain wind speed which is the cut-in wind speed to create a starting torque for it to rotate and generate electricity. For VAWT, research show that in order to create the maximum ratio of the lift force to the drag force (L/D ratio) of the blade, the streamline of the wind need to be in direction of the optimum angle of attack for the wind turbine blade (Chong et al., 2013a). Although for VAWT, wind can come from any angle, but not all the blade can always create the maximum L/D ratio. Different rotational position, the blade will create different lift and drag force.

In order to increase the efficiency of the wind turbine, there are many researches have been done on modify and design of the wind turbine. According to Bhutta (2012),

there are several configuration of VAWT. For the Darriues type of wind turbine, some innovative designs like Egg-beater type Darriues wind turbine, Giromill turbine which using straight blade to operate, Variable geometry oval trajectory (VGOT) Darriues turbine, Darriues-Masgrowe rotor, Twisted three bladed Darieus rotor and Crossflex wind turbine are created for higher energy generation. Besides Darrieus turbine, there are research to combine Savonius rotor with Darrieus rotor and two lead semi rotary VAWT (Aslam Bhutta et al., 2012).

Kim & Gharib (2013) conducted research on additional of flat deflector on the VAWT, and result show that the output power is increased which is dependent on the width and height of the deflector (Kim & Gharib, 2013). Islam et al. (2013) imply the "Fish Schooling Concept" in the VAWT farm, the output energy is about 10 times more compare to HAWT (M. R. Islam, Mekhilef, & Saidur, 2013). McTavish et al. (2012) developed a novel VAWT which is an asymmetric vertically-stacked stages turbine, experiment conducted show the design increase average static torque (McTavish, Feszty, & Sankar, 2012).

1.3 Urban building integrated with wind turbine

Urban wind turbine development is getting popular in some of the main city in the world. Some of the example buildings are shown in figure 1.1, 1.2 and 1.3. The main advantages for this building integrated wind turbine are it utilising the natural wind energy resources, better power distribution, and the economic exploitation of roof top of the building (Toja-Silva et al., 2013).

Figure 1.1: Bahrain World Trade Centre (http://www.bahrainwtc.com/, 12/06/13)

Figure 1.2: Bolte Bridge (Toja-Silva et al., 2013)

Figure 1.3: Darrieus wind turbine installed on building (Sharpe & Proven, 2010)

Toja-Silva et al. (2013) conducted research on the urban wind energy exploitation system. In the research, it show that the HAWT is more suitable for flat-terrain area rather than in urban area, due to the wind turbulence intensity and multidirectional from the presence of building (Toja-Silva et al., 2013).

Because of the unsteady wind flow, some of the commercial urban area VAWT utilize stator vane to further increase the efficiency of the wind flow on the angle of attack to the blade. Sistan wind mill which is driven by drag force with additional of wing wall, top and bottom disk increase the efficiency of the turbine (Müller, Jentsch, & Stoddart, 2009). Similarly, Yao et al. (2013) using a drag driven VAWT with additional of a tower cowling which consists of eight baffles plates distributed axially to the wind turbine can prevent the turbine create negative torque (Yao, Tang, & Wang, 2013). The Zephyr turbines which use the stator vane to reduce the turbulence show improvement for the turbine (Pope et al., 2010).

According to Chong et al. (2013) where the research conducted building integrated wind turbine, the performance of the VAWT can be improved by utilize of omni-direction guide vane (ODGV). By considering aerodynamics in the design of the

guide vane, it can lower down the cut in speed for the wind turbine, therefore longer working hour for the VAWT and increase the output. The concept of Chong's design is to reduce the negative torque created on the lift type turbine blade by the ODGV. The design can be integrated to the urban building to create a green building, where power generated by the VAWT will be used by the building and reduce the power consumption of the building. Figure 1.4 below show the illustrative view of the installation of ODGV on a high rise building (Chong et al., 2013a; Chong, Fazlizan, Poh, Pan, & Ping, 2012).

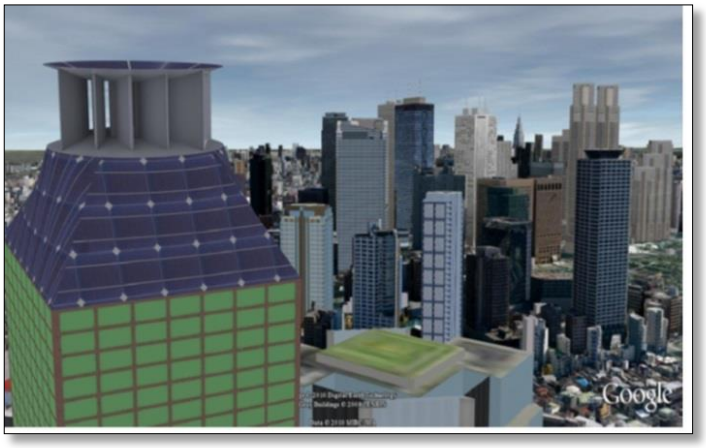

Figure 1.4: Illustrative view of high-rise building with the hybrid renewable energy system integrated on it (Chong, Naghavi, Poh, Mahlia, & Pan, 2011)

The present research will involve the design and flow simulation of a power-augmented shroud for urban wind turbine system adopt the working principle of Chong's research and further increase the efficiency of VAWT by designing the shroud to create a better angle of attack for the VAWT and reduce the drag which deplete the efficiency of the wind turbine.

1.4 CFD simulation

In both industrial and non-industrial application, computational fluid dynamics (CFD) is a popular and powerful tool to solve problem related to fluid flow by using numerical analysis. There are several popular commercial software like ANSYS, OpenFOAM, Flovent, CFdesign, COSMOS-Floworks, STAR-CD etc. which can perform analysis of the three dimension, heat transfer and time dependent turbulence flow (Mohamed, 2012). The fluid flow physical characteristic is solved and analysis by the calculation of the fundamental flow equation, which is based on Navier-Stokes equation. Generally, there are three major steps in CFD which are pre-processing, solving, and post processing. In the preprocessing, the geometry is defined and the volume of the fluid is divided to small elements which named as mesh. All the physical properties of the fluid like density, viscosity, enthalpy etc. as well as the boundary condition need to be input before the solver compute the iteratively calculation as a steady-state or transient. Finally the post processing will show all the result of the analysis in graphical method. Finite difference method (FDM), finite volume method (FVM) and finite element method (FEM) are the main discretization method in the solver (Roy & Saha, 2013).

1.5 Objective of Study

This study embarks on the following objectives:

i) To study the aerodynamic characteristic for VAWT

ii) To design power augmented shroud for VAWT.

iii) To simulate the fluid flow of the power augmented shroud by computational fluid dynamics (CFD) simulation-ANSYS FLUENT 14.0.

iv) To analysis, compare and validate the simulation result with other research.

CHAPTER 2 LITERATURE REVIEW

From the first law of thermodynamics, it stated that energy cannot be created nor destroyed; it only can convert to different form of energy. Wind turbine extract energy from the wind kinetic energy to mechanical and electrical energy which transmit by the main grid. The power from the wind stream can be represented as following:

$$P = \frac{1}{2}\dot{m}v^2 \tag{2.1}$$

where v is the wind stream velocity.

Let the wind stream pass through a cross section, p, and the air density, $\dot{m}$, the mass flow rate of the wind stream is

$$\dot{m} = pAv \tag{2.2}$$

Substitute equation (2.2) into equation (2.1),

$$P = \frac{1}{2}pAv^3 \tag{2.3}$$

2.1 Axial momentum theory

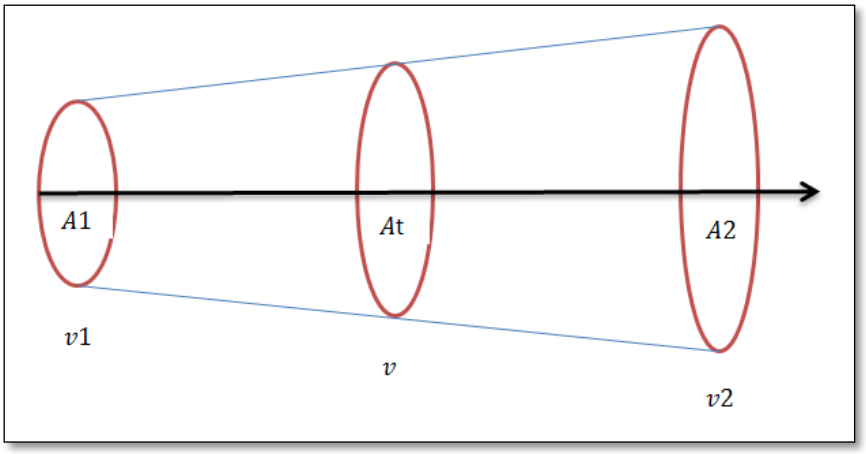

Figure 2.1: The axial stream tube model

Consider a wind stream tube where the wind turbine rotor at the center with the swept area of At, and the aero direction denote the wind stream direction. According to the conservation of mass, the mass flow rate at $A1$, At and $A2$ is same (Asress, 2013).

$$\dot{m}1 = \dot{m}t = \dot{m}2 = \dot{m} \tag{2.4}$$

The thrust force experienced by the wind turbine can be written as:

$$F = \dot{m}.(v1 - v2) \tag{2.5}$$

The power extract from the wind turbine is denoted by

$$P = F.v \tag{2.6}$$

When substitute equation (2.2) and (2.5) into (2.6),

$$P = p.A.v^2 .(v1 - v2) \tag{2.7}$$

By the law of conservation of energy, from equation (2.1)

$$P = \frac{\Delta E}{\Delta t} = \frac{1}{2}.\dot{m}.(v1^2 - v2^2) \quad (2.8)$$

$$P = \frac{1}{2}.p.At.v.(v1^2 - v2^2) \quad (2.9)$$

By equal the equation (2.7) and (2.9)

$$P = \frac{1}{2}.p.At.v.(v1^2 - v2^2) = p.At.v^2.(v1 - v2) \quad (2.10)$$

$$\frac{1}{2}.(v1^2 - v2^2) = v.(v1 - v2) \quad (2.11)$$

$$v = \frac{1}{2}.(v1 + v2) \quad (2.12)$$

From (2.8)

$$P = \frac{1}{2}.\dot{m}.(v1^2 - v2^2) \quad (2.13)$$

$$= \frac{1}{2}.p.At.v.(v1^2 - v2^2) \quad (2.14)$$

By substitute (2.12) into (2.14)

$$\text{P} = \frac{1}{4}.p.At.(v2 + v1).(v1^2 - v2^2) \quad (2.15)$$

$$= \frac{1}{4}.p.At.v1^3.\left(1 + \left(\frac{v2}{v1}\right) - \left(\frac{v2}{v1}\right)^2 - \left(\frac{v2}{v1}\right)^3\right) \quad (2.16)$$

By differentiation, $\dot{E}$ respect to $\frac{v2}{v1}$, the maximum power for the wind turbine occur when the $\frac{v2}{v1} = \frac{1}{3}$, therefore

$$Pmax = \frac{16}{27}.\frac{1}{2}.p.At.v1^3 \quad (2.17)$$

The coefficient of power, Cp, is equal to

$$P = Cp.\frac{1}{2}.p.At.v1^3 \quad (2.18)$$

$$Cp = \frac{P}{\frac{1}{2}.p.At.v1^3} \quad (2.19)$$

$$Cp, max = \frac{16}{27} = 0.593 \quad (2.20)$$

The maximum value of power coefficient is approximately 0.593. The limit of this power coefficient is known as Betz limit.

2.2 Tip speed ratio (TSR)

Normally the rotational speed for the wind turbine is measured in either revolution per minute (rpm) or radians per second (rad/s). There is another measurement for wind turbine which is the tip speed, the tangential speed of the rotor.

$$U = \omega R \quad (2.21)$$

The ratio for the tip speed over the undisturbed wind stream velocity, $v0$, is the tip speed ratio, λ

$$\lambda = \frac{\omega R}{vo} \tag{2.22}$$

Where

ω = angular velocity (rad/s)

R = rotor radius (m)

vo = undisturbed wind speed (m/s)

2.3 Aerodynamic Model of Lift type VAWT

When wind stream blow through the wind turbine, difference pressure will be created on the surface of the blades. This different in pressure will create the lift and drag force which are in perpendicular direction. The magnitude for this lift and drag forces depend on the direction and velocity of the wind stream, the shape of the blade and the orientation. The angle where the resultant wind force meets with the chord length of the blade is named as angle of attack (AOA). Figure 2.2 show the velocity and force vector of VAWT.

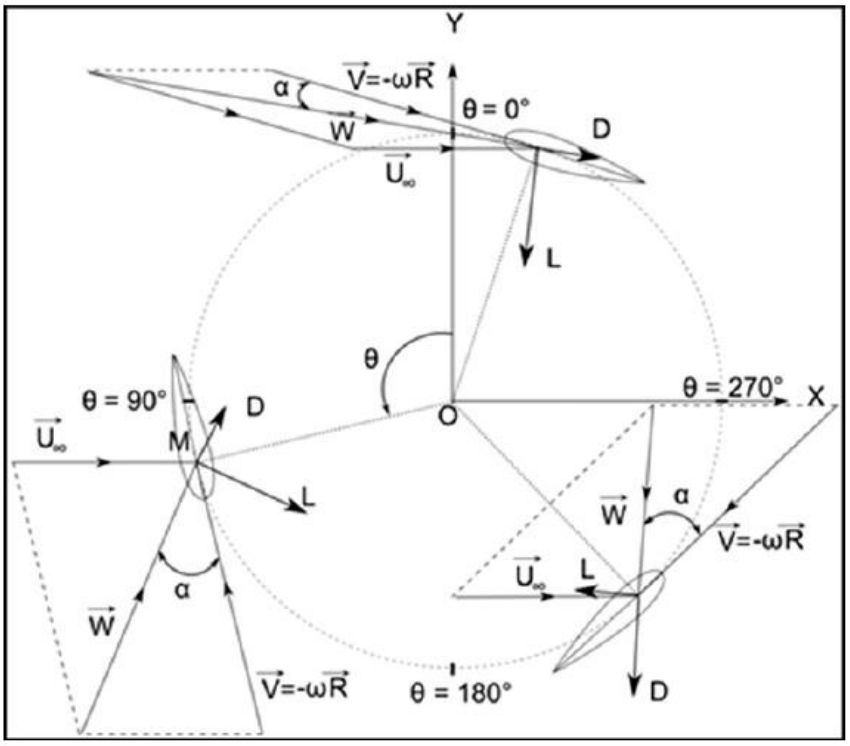

Figure 2.2: Forces and velocities distribution for VAWT (Maître, Amet, & Pellone, 2013)

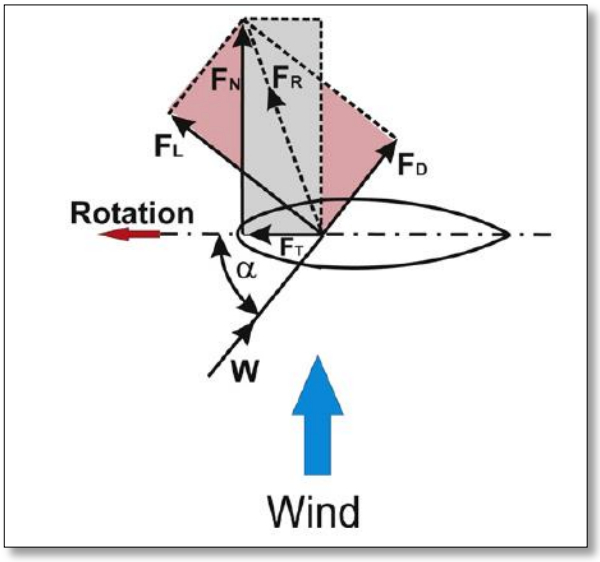

Figure 2.3: Forces and velocities distribution on VAWT blade (Mohamed, 2012)

The drag force is the component parallel to the angle of attack (AOA) of the wind whereas the lift force is perpendicular to the resultant wind direction. The resultant

force,Fr, can be resolved to two components which are tangential force, Ft, and normal force, Fn. The tangential force is the component to create torque for the wind turbine where

$$T = Ft.R \tag{2.23}$$

Where T = torque generated

The torque drive the wind turbine to rotate, hence generate power. The lift type VAWT is aerodynamic complex where

a) The incoming wind and the moving of the blade create local relative flow velocity, W
b) The resultant forces from the lift and drag force is resolved to be tangential and normal forces.
c) At different orientation and position of the blade will have different value of the forces
d) Total of the local torque from each blade to generate the power of the VAWT

2.3.1 Rapid Change of local angle of attack

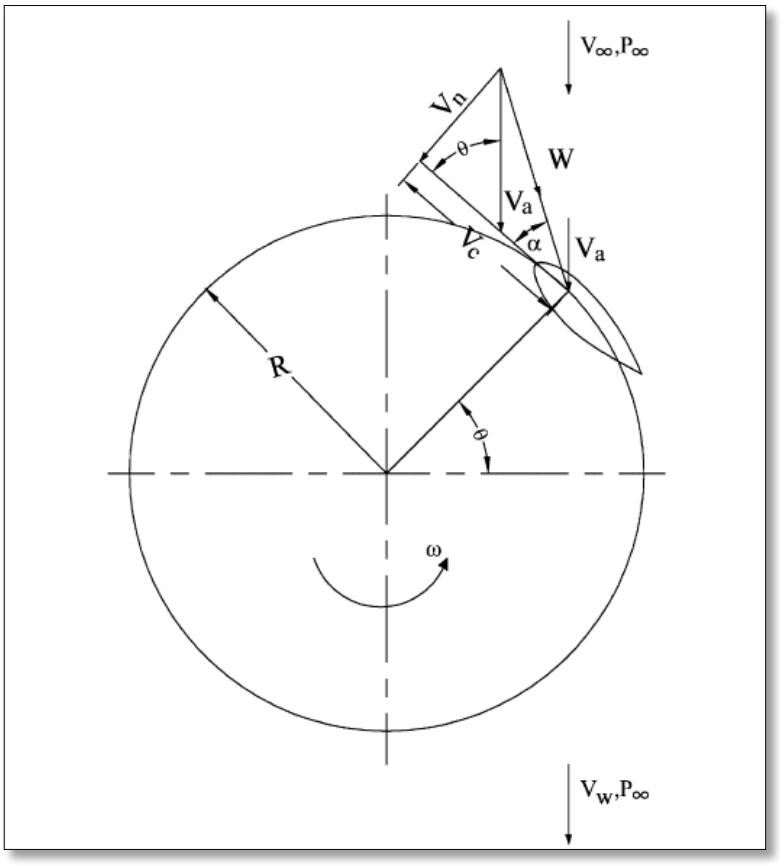

Figure 2.4: Flow velocities of straight-bladed Darriues- type VAWT (M. Islam, Ting, & Fartaj, 2008)

The angle of attack for the blades is always change from the upstream and downstream of the wind where it is occur in the axial direction for the VAWT. The mathematic expression for the velocities as following (Asress, 2013):

$$Vc = R\omega + Va\cos\theta \tag{2.24}$$

$$Vn = Va\sin\theta \tag{2.25}$$

Where

Vc = chordal velocity component

Vn = normal velocity component

Va = induced flow velocity

θ = azimuth angle

The angle of attack ($\propto$), can be written as following:

$$\propto = tan^{-1}\left(\frac{Vn}{Vc}\right) \tag{2.26}$$

$$\propto = tan^{-1}\left(\frac{Va\sin\theta}{R\omega + Va\cos\theta}\right) \tag{2.27}$$

$$\propto = tan^{-1}\left(\frac{\sin\theta}{\left(\frac{R\omega}{V\infty}\right)\left(\frac{V\infty}{Va}\right) + \cos\theta}\right) \tag{2.28}$$

2.3.2 Variation of local relative flow velocity, W

From figure 2.4 also, the relative flow velocity, W can be expressed as

$$W = \sqrt{(Vc)^2 + (Vn)^2} \tag{2.29}$$

By substituting equation 2.24 and 2.25 into 2.29, the non-dimensional velocity ratio can be written as following:

$$\frac{W}{V\infty} = \frac{W}{Va}.\frac{Va}{V\infty} = \frac{Va}{V\infty}\sqrt{\left[\left(\frac{R\omega}{V\infty}\right).\left(\frac{V\infty}{Va}\right) + \cos\theta\right]^2 + sin^2\theta} \tag{2.30}$$

2.3.3 Rapid Change of Tangential Force and Normal Force

From figure 2.3, it is shown that the lift and drag forces can be resolved to be tangential and normal components. The tangential force coefficient, Ct and the normal force coefficient, Cn, basically is the difference between the lift and drag forces as following:

$$Ct\ (\theta) = Cl \sin\alpha - Cd \cos\alpha \tag{2.31}$$

$$Cn\ (\theta) = Cl \cos\alpha - Cd \sin\alpha \tag{2.32}$$

The net tangential and normal forces are

$$Ft\ (\theta) = 0.5\ .Ct.p.c.H.W^2 \tag{2.33}$$

$$Fn\ (\theta) = 0.5\ .Cn.p.c.H.W^2 \tag{2.34}$$

Where

c = the blade chord

H = height of the turbine

2.3.4 Computation of Averaged Tangential Force and Normal Force, Torque and Power

The average tangential force, $Ft\ avg$ and average normal force, $Fn\ avg$, can be expressed in a function of azimuth angle, θ, for a complete revolution.

$$Ft\ avg = \frac{1}{2\pi}\sum_{\theta=0}^{2\pi} Ft\ (\theta) \tag{2.35}$$

$$Fn\ avg = \frac{1}{2\pi}\sum_{\theta=0}^{2\pi} Fn\ (\theta) \tag{2.36}$$

The total torque and power generated for the VAWT can be obtained as

$$\tau = N.R.Ft\ avg \tag{2.37}$$

$$P = \tau.\omega \tag{2.38}$$

Where

N= number of blade for VAWT

2.4 Urban area wind speed

The wind speed for urban area is lower than the flat terrain, for the urban area wind profile is highly depending on the height of the building and the positioning, where the presence of the adjacent building can cause wind shadow and the turbulence intensity and the multi-directionality increase severely (Toja-Silva et al., 2013; Walker, 2011). According to Walker (2011), the urban wind speeds within the planetary boundary can be represented by the following equation (Walker, 2011):

$$\bar{u}(z) = \frac{u*}{k} Ln\ (\frac{z-d}{zo}) \tag{2.39}$$

Where

u* = Friction velocity

k = von Karman's constant

zo = roughness length

d = displacement height

$\bar{u}(z)$ = acerage wind speed at height z above ground.

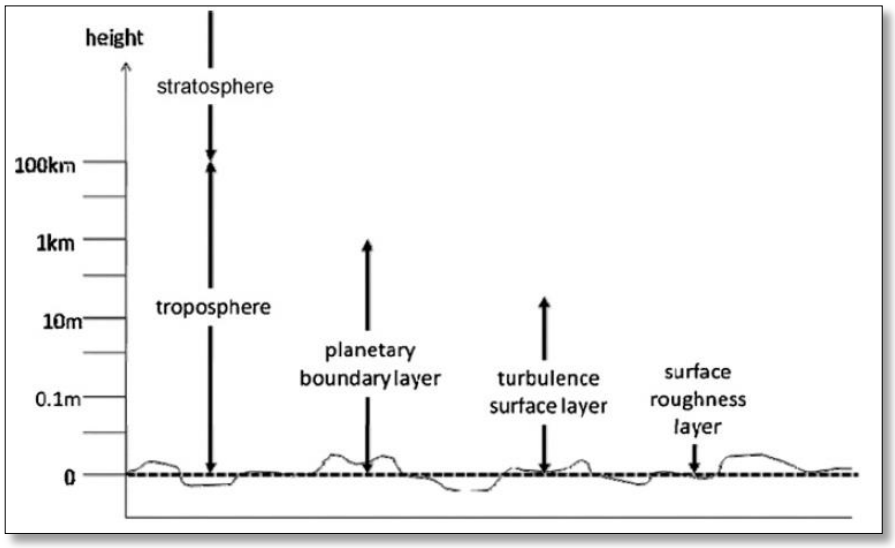

Figure 2.5: Vertical layers of the atmosphere (Walker, 2011)

The equation above is applicable for the height above 2h from ground, where h is the roughness obstacle height. For the wind speed within the surface roughness layer, where the height is less than 2h, the relation is written as:

$$Uh = \frac{\alpha u*}{k} Ln\left(\frac{h-d}{zo}\right) \quad (2.40)$$

Where

α = wake factor

Uh = Wind speed at height, h

Several research found that the wind velocity and the turbulence intensity is strongly influenced by the by the roof profile as well (Toja-Silva et al., 2013). From Ledo et al. who carry out research on four types of roof which are flat, sloped, pitched and pyramidal roofs. The result shows that flat roof give the best flow velocity distribution and less turbulence intensity, thus it can yield higher and more consistent power compare to others roof profile. For sloped roof also can obtain high wind velocities and low turbulence intensity by installed the wind turbine at the top edge

(Ledo, Kosasih, & Cooper, 2011). Similarly, Abohela et al. (2013) showed that the vaulted roof show the best electricity yield among flat, wedged, domed, vaulted, gabled, and pyramidal roof. Whereas, the wedged rood show the least wind accelerate result (Abohela, Hamza, & Dudek, 2013).

2.5 Shrouded Vertical Axis Wind Turbine

The efficiency of the VAWT is always the main concern where all researchers aim to improve. Over the years there are many innovative design of the VAWT including the use of shroud to increase the total power generated.

According to Yao et al. using 8 baffles blades evenly distributed to the drag type Savonius VAWT in the cowling tower, the research show that the design increase the power coefficient by increase the wind speed reaching the wind turbine and reduce the negative torque by adjusting the wind direction (Yao et al., 2013).

Similar to Müller et al., their research adapt an old form of wind energy converter in modern building integration as shown in figure 2.6. The design can increase the theoretical efficiency about 48% and the optimistic state up to 61% (Müller et al., 2009).

Ducted wind turbine which introduce by Grant et al. install the wind turbine at the edge of the building's roof which improve the power coefficient higher than the Betz limit. However, the main drawback for the design is the wind turbine can only operate with the wind direction perpendicularly (Toja-Silva et al., 2013).

As shown in figure 2.7 is the Zephyr turbine which design by Pope et al. The turbine use stator vanes distributed evenly with reversed winglets. The in-coming wind will enter the ring of stator blades which direct the wind to leave at particular angle of attack and strike with the Savonius rotor hence increase the power generated. This stator blade reduce the turbulence flow hence decrease the aerodynamic loading on the blade.

The optimum TSR for this design is 0.4, when the wind further increase the TSR, the Cp obtained will be reduced (Pope et al., 2010).

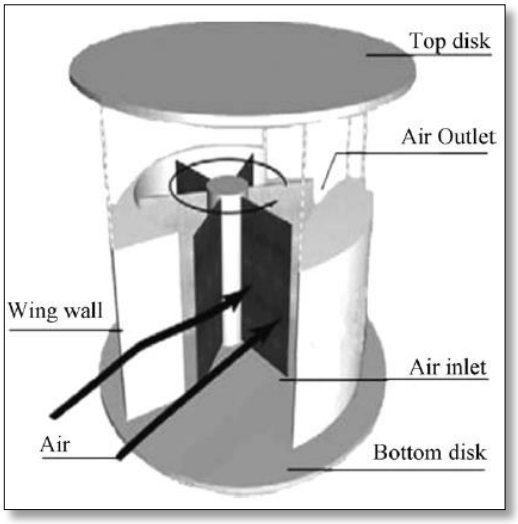

Figure 2.6: Sistan wind mill (Müller et al., 2009)

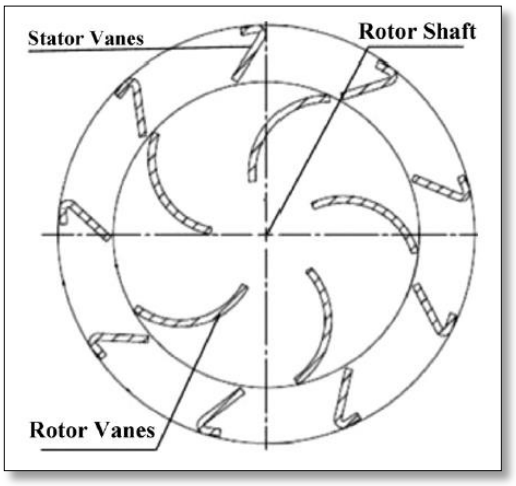

Figure 2.7: Zephyr turbine (Aslam Bhutta et al., 2012)

For Chong et al. (2013a) research on the omni-directional power augment guide vane (PAGV) which is a hybrid renewable energy system consists solar power generation and rain water collector for urban high rise building. The system utilise the PAGV which surrounds the VAWT that orients the air inlet and wind speed to the

blades. It shows that the improvement on the self-starting behaviour where it lower down the cut in speed with the omni-direction PAGV, hence the working hour will be increase. The rotor speed is increased as much as 182% and the power output is increased by 3.48 times at the peak torque. The design of the vane can minimize the negative torque created on the lift type wind turbine (Chong et al., 2013a; Chong et al., 2012; Chong et al., 2011; Chong et al., 2013b).

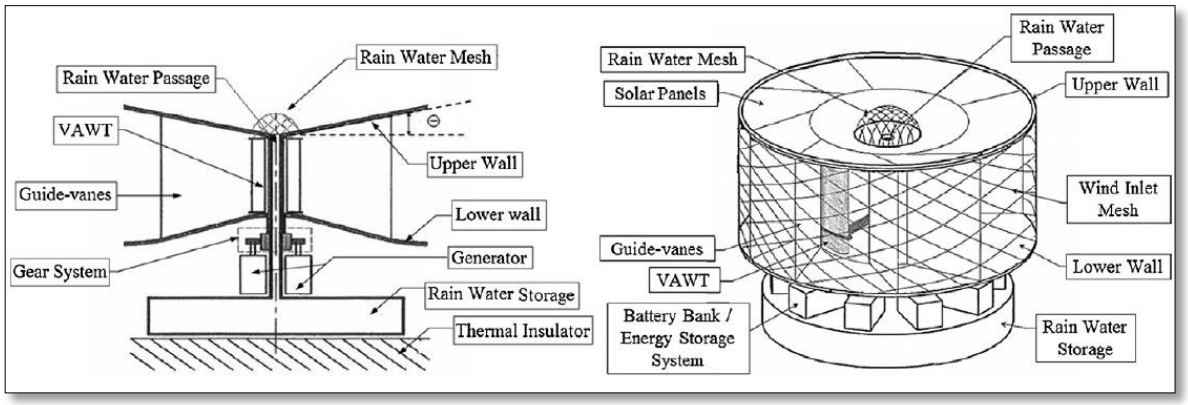

Figure 2.8: General arrangement of the novel omni-direction-guide-vane integrated system (wind-solar hybrid energy system with rain water collection integrated)

2.6 Numerical Method and model

Computational Fluid Dynamics (CFD) is a study of fluid mechanics which uses numerical analysis of the complex fluid flow. The Navier-Strokes equation is the fundamental basis of most of the CFD problem which govern the motion of a Newtonian viscous fluid since century ago (Mohamed, 2012).

For an incompressible flow, the velocity and the pressure are resolved from the conservation of mass of the Navier-Strokes equations can be written as ("ANSYS FLUENT 12.0, Theory Guide," 2009):

$$\frac{\partial \rho}{\partial t} + \nabla . (\rho . \vec{v}) = Sm \qquad (2.41)$$

Where Sm = source term

This equation is the general form of the mass conservation equation and is valid for both incompressible and compressible flow. The source term is the mass added to the continuous phase from the dispersed second phase and any user-defined sources.

The conservation of momentum in an inertial reference frame can be written as:

$$\frac{\partial \rho}{\partial xi}(\rho.\vec{v}) + \nabla.(\rho.\vec{v}.\vec{v}) = -\nabla.p + \nabla.\left(\bar{\bar{T}}\right) + \rho.\vec{g} + \vec{F} \qquad (2.42)$$

Where

p = static pressure

$\bar{\bar{T}}$ = Stress tensor

$\rho.\vec{g}$ = gravitational body force

$\vec{F}$ = external body forces

The stress tensor, $\bar{\bar{T}}$ is given by

$$\bar{\bar{T}} = \mu.\{(\nabla.\vec{v} + \nabla.\vec{v}^{T}) - \frac{2}{3}.\nabla.\vec{v}I\} \qquad (2.43)$$

Where

μ = molecular viscosity

I = unit tensor

2.6.1 Turbulence Model

In the CFD community, there are three most popular turbulence models which are Direct Numerical Simulation (DNS), Large Eddy Simulation (LES) and Reynolds-Averaged Navier-Strokes (RANS). Among these models, the RANS model is adopted for 2D numerical simulation, the DNS model involve large amount of computation and time, whereas, LES is more suitable for the 3D simulation (Nobile, 2011; Wang, Ingham, Ma, Pourkashanian, & Tao, 2010).

RANS model is the oldest approach for turbulence modelling. It governs the transport of the averaged flow quantities, with the whole range of the scales of turbulence being modelled. RANS-based model approach therefore greatly reduces the required computational effort and resources, and widely adopted for practical engineering applications. It often used to compute time-dependent flow, whose unsteadiness may be externally imposed or self-sustained ("ANSYS FLUENT 12.0, Theory Guide," 2009).

There are many option of the turbulence model available in ANSYS FLUENT include Spalart-Allmaras model, k-ε model, k-ω model, k-kl-ω transition model, Transition SST model, Reynolds Stress Model (RSM), Detached Eddy Simulation (DES), and Large Eddy Simulation (LES) model ("ANSYS FLUENT 12.0, Theory Guide," 2009).

Among these models, the Spalart-Allmaras (SA) model is a simple one equation turbulence model, the near wall gradients of the transported variable is smaller than the k-ε turbulence kinetic energy equation. Therefore it might not be so sensitive at the near wall treatment for the blades of VAWT. The standard k-ε model is more suitable when the flow is fully turbulent and gives a better analysis result compare to SA model. Renormalization of the k-ε model which known as RNG k-ε turbulence model can improve the accuracy for swirl flow significantly. The shear stress transport (SST) k-ω

turbulence model is a two equation eddy viscosity model gives advantage for the near wall and far field region with different formulation (Roy & Saha, 2013).

2.6.2 Shear Stress Transport (SST) k-ω turbulence model

Menter developed The Shear- stress transport (SST) k-ω model. This model blends the accurate formulation of the k-ω model at the near-wall region with the free stream independence of k-ε model at the far field, by convert the k-ε model into k-ω formulation. This SST k-ω model, further improve the k-ω model by some refinement as following("ANSYS FLUENT 12.0, Theory Guide," 2009):

i) A blending function is multiplied with the standard k-ω model and k-ε model, and both added together. This blend function enable activates the standard k-ω model when it is near wall region and activates the k-ε model when zero away from the surface.

ii) The SST model incorporates a damped cross-diffusion derivative term in the ω equation.

iii) To account the transport of the turbulence shear stress by modify the turbulence viscosity.

iv) The modelling constants are different.

v) Addition of cross-diffusion term in the ω equation and a blend function in order to make the model equation behave correctly in both far field and near wall zones.

These refinements make the SST k-ω model become more accurate and reliable than the standard k-ω model.

The SST k-ω model has a similar form to the standard k-ω model:

$$\frac{\partial}{\partial t}(\rho.k) + \frac{\partial}{\partial xi}(\rho.k.ui) = \frac{\partial}{\partial xj}\left(\Gamma k.\frac{\partial k}{\partial xj}\right) + \tilde{G}k - Yk + Sk \quad (2.44)$$

And

$$\frac{\partial}{\partial t}(\rho.\omega) + \frac{\partial}{\partial xi}(\rho.\omega.ui) = \frac{\partial}{\partial xj}\left(\Gamma\omega.\frac{\partial \omega}{\partial xj}\right) + G\omega - Y\omega + D\omega + S\omega \quad (2.45)$$

Where

$\tilde{G}k$ = generation of turbulence kinetic energy due to mean velocity gradient

$G\omega$ = generation of ω

Γk = effective diffusivity of k

$\Gamma\omega$ = effective diffusivity of ω

Yk = dissipation of k

$Y\omega$ = dissipation of ω

$D\omega$ = cross-diffusion term

Sk , $S\omega$ = user defined source terms

2.6.3 Sliding Mesh

Sliding mesh is the function in the CFD software that used to compute the unsteady flow case which involves time accurate solution for rotor-stator interaction. This method is the most accurate method for simulate flow for multiple moving reference frames, however, it is very computationally demanding. Many cases involve unsteady solution for the sliding mesh is time periodic which the solution repeats with period related to the speeds of the moving domain. The concept of this method allows two or more adjacent meshes to move relatively in each other, and the flow flux will cross the mesh interface.

When using this method, two or more cell zone is needed, and each cell zone must be bounded by at least one interface, where it meets with other opposing cell zone.

The “mesh interface” associates the interface zone with the adjacent cell zone. This “mesh interface” allows two or more cell zone move relatively to each other in each discrete step. The mesh interface can be in any shape, as long as the interface boundaries having the same geometry. During the rotational or translational motion, the node alignment along the mesh interface is not required; however the time dependent solution is needed for the unsteady flow ("ANSYS FLUENT 12.0, Theory Guide," 2009).

2.6.4 Y+ value

The y^+ value are dependent on two factors which are the Reynolds number of the flow and the resolution of the mesh. It is a non-dimensional parameter defined only in wall-adjacent cell as following("ANSYS FLUENT 12.0, Tutorial Guide," 2009):

$$y^+ = \frac{y}{\mu}.\sqrt{\rho.\tau w} \tag{2.46}$$

where

τw = wall shear stress

τw = distance from the wall to the cell center

μ = molecular viscosity

ρ = density of the fluid

The mesh need to have a y^+ value approximately to one, so that the laminar and the transitional boundary layers can be captured correctly. If the y^+ value is too large which about more than 5, the transition onset location move upstream with increasing of y^+ value. The bounded second order upwind base on discretization for the turbulence,

mean flow and transition equations is recommended to be used ("ANSYS FLUENT 12.0, Theory Guide," 2009).

According to Maître et al. (2013), the laminar, buffer and turbulence layers can be defined by the y+ value range. For the laminar layer, $y+ < 5$, for the buffer, $5 < y+ < 30$, whereas for the turbulence layers, $30 < y+ < 300$ (Maître et al., 2013).

CHAPTER 3 METHODOLOGY

3.1 Design of Omni Directional Guide Vane

According to previous research by Chong et al. (2013a), an Omni-Directional Guide Vane (ODGV) which is a circular patterned design, integrated with VAWT to capture the wind energy from four main directions as shown in figure 3.1 below. With this ODGV, the wind turbine able to increase the performance by optimizing the incoming wind speed, channel the wind flow to make a better angle of attack to the blades of the VAWT. By experiment, it shows that utilizing the ODGV, it improves the self-starting of the wind turbine where the output at maximum torque is 3.48 times comparing to bare VAWT (Chong et al., 2013a).

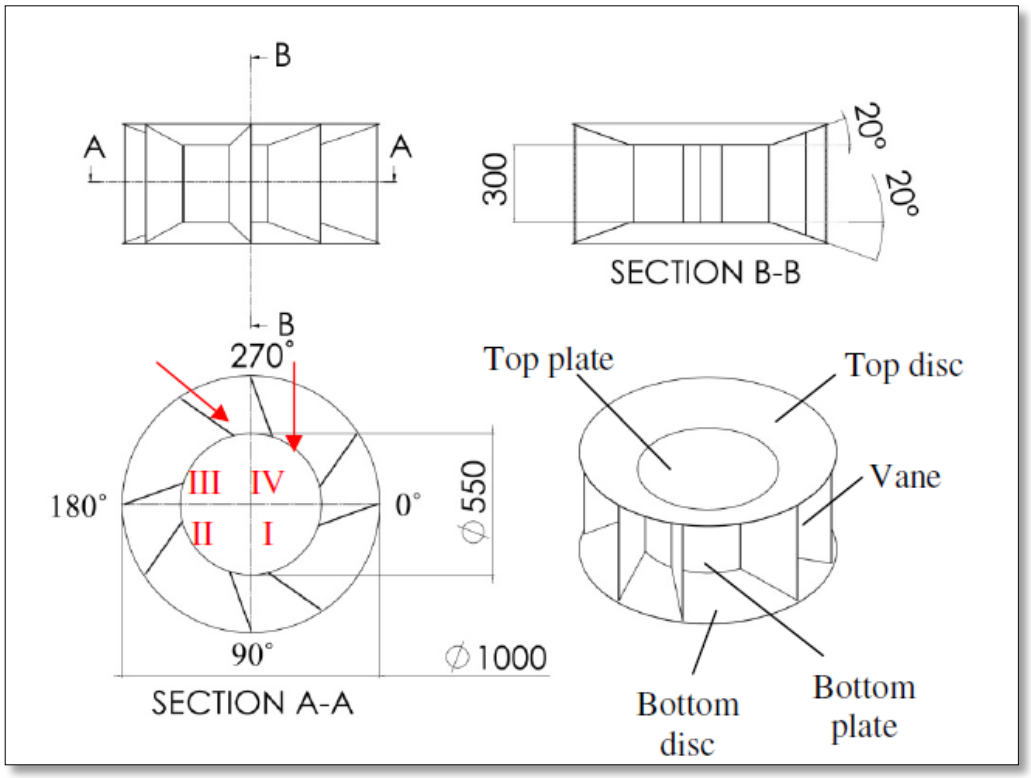

Figure 3.1: General layout of the ODGV (Chong et al.)

In this project, the aim is to redesign the power augmented shroud which identified as new omni-directional guide vane design so that the wind flow will be smooth when go through the system; hence it can further increase the coefficient of

torque followed by the coefficient of power. Compare the original design of ODGV from Chong et al. as shown in figure 3.2 with the new ODGV design in figure 3.3. The similarity is there are totally four pairs of guide vane at azimuth angle of 0^o, 90^o, 180^o, and 270^o, and each pairs of the guide vane is tilted at angle 20^o, and 55^o, and the outer dimension of the ODGV is twice of the VAWT rotor diameter.

For this new design ODGV, the guide vanes are divided into two pieces with same length. The inner and outer tips of the guide vane remain same location and there is a 10^o angle tilted from the original guide vanes as shown in figure 3.3 below. The detail drawing for the new ODGV design is shown in Appendix A.

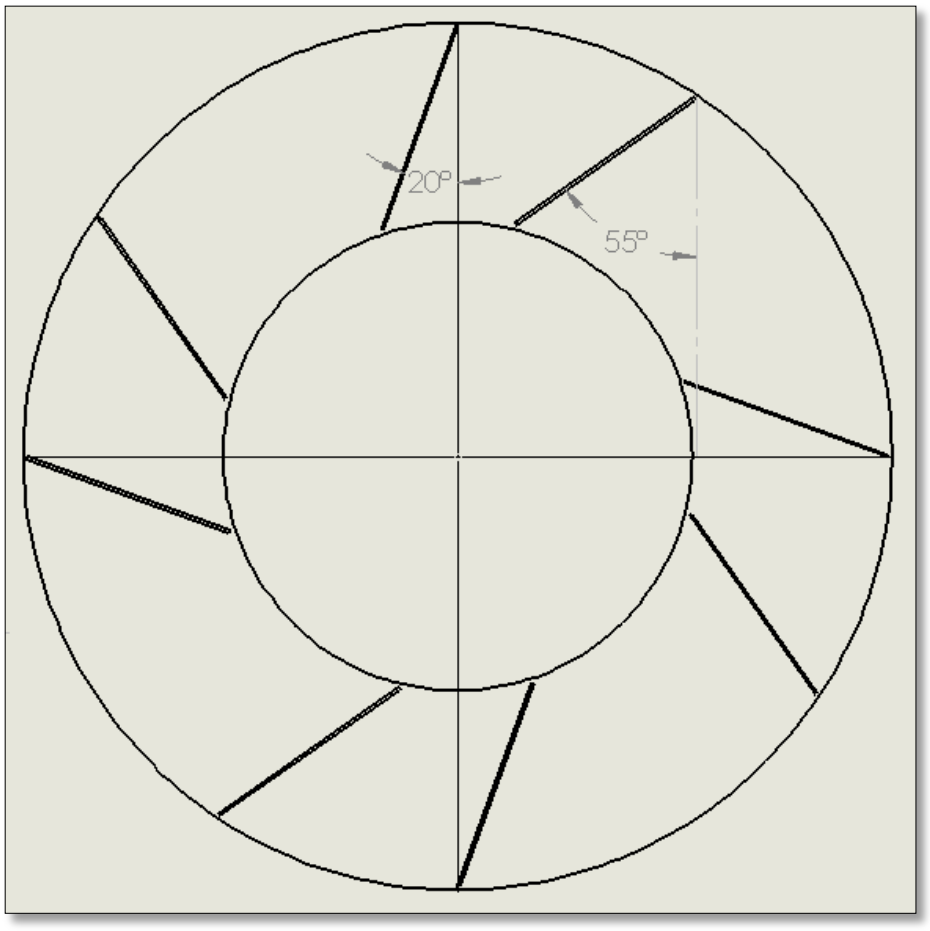

Figure 3.2: Original ODGV design (Chong et al., 2013a)

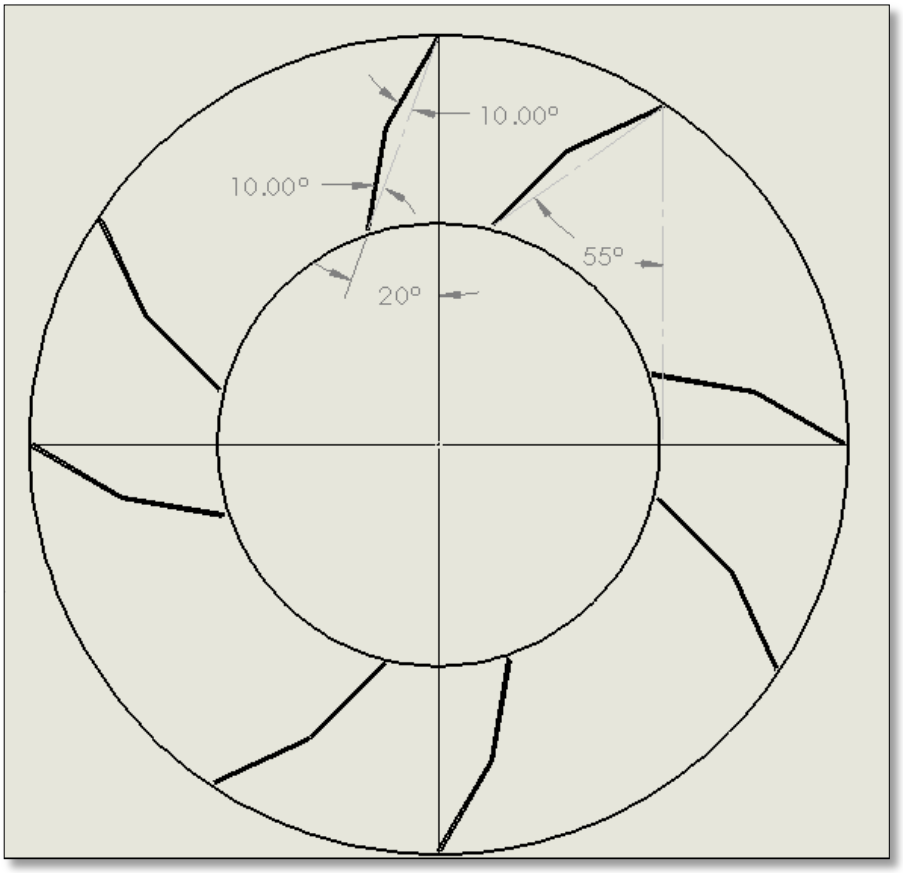

Figure 3.3: New ODGV design

3.2 Numerical Flow Simulation

In this project, the 2D simulation of the VAWT is conducted by using the commercial CFD software ANSYS FLUENT 14.0 as the solver. ANSYS FLUENT is one of the most popular commercial CFD software which enables the user to simulate the fluid mechanics, fluid flow, heat and mass transfer as well as the phenomena which involve turbulence, reacting, and multi-phase flow (Mohamed, 2012). This software offer different types of simulation module for both steady and unsteady flow. ANSYS FLUENT is based on the finite volume method (FVM) that discretizes the computational domain into small elements and has been verified in many applications (Li, Zhu, Xu, & Xiao, 2013). The main reason of using CFD method is the time and cost saving.

The simulation is verified by re-simulate the NACA 0015 airfoil single bladed VAWT which accomplished by Oler et al. published by Sandia National Laboratories. Besides, the simulation for ODGV also verified and compared with Chong et al. simulation (Oler, 1983).

According to Oler's experiment, a straight-one-bladed rotor with NACA 0015 was built and operated in a water tow tank with 10 meters length, 5meters width and 1.25 meters depth. The chord to radius (C/R ratio) value is 0.25, and the experiment conducted by using water as working fluid that facilitate relatively low frequency measurements while working at appropriate blade Reynolds numbers. Besides, the blade forces and pressures are more easily to be measured. The summary of the experiment data as following (Oler, 1983):

Table 3.1: Oler's experiment parameter

Parameter	**Value**
Airfoil	NACA 0015
Chord length ,c (m)	0.1524
Rotor tip speed , R ω (m/s)	0.457
Reynolds number, Re	67,000
Towing speed (m/s)	0.091
Rotor diameter, D (m)	1.22
Rotor radius, R (m)	0.61
Tip speed ratio, TSR	5.1

3.3 Geometry Modelling

The symmetrical airfoil NACA 0015 is one of the common use blade sections in VAWT. The airfoil and the domain geometry are modelled by the DesignModeler software which is a package with the ANSYS 14.0. Figure 3.4 below show the unit size geometry of NACA 0015. The detail coordinate for NACA 0015 is tabulated in Appendix B.

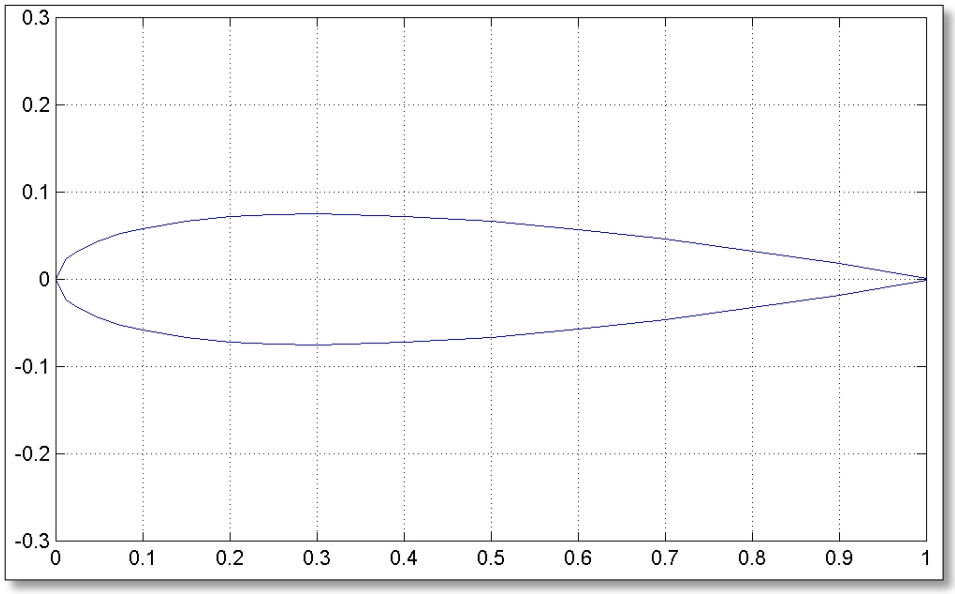

Figure 3.4: NACA 0015 (http://airfoiltools.com/airfoil/details?airfoil=naca0015-il, 12/06/12)

Totally there are two geometry models are drawn which are the VAWT space and the tunnel space. For the VAWT space it consists of the single blade NACA 0015 airfoil with chord length 0.1524 m and the distance from the origin is 0.61 m. The VAWT space is divided to 3 regions, which are the airfoil space, subgrid, and the main grid. Whereas for the tunnel is modelled according to the dimension as the Oler's experiment. The design of the ODGV is located at the tunnel space. Figure 3.5 and figure 3.6 show the sketches of the VAWT space and the tunnel space.

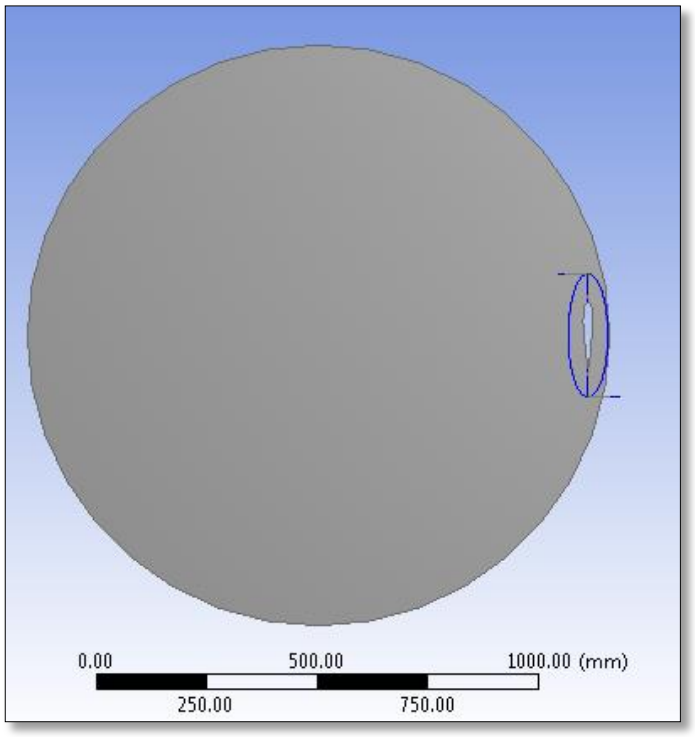

Figure 3.5: VAWT space

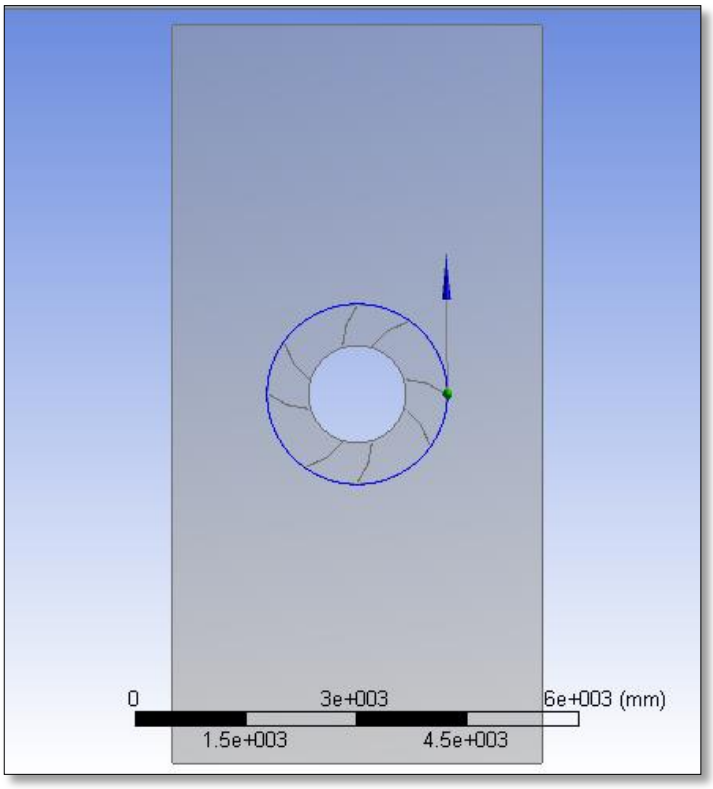

Figure 3.6: Tunnel space

3.4 Computational Mesh

Basically, in order to do simulation using the sliding mesh function, there is two or more mesh files need to be created. For this simulation, the mesh is created with the mesh function in the ANSYS software. There are two mesh files which are identified as the “airfoil” that constructed from the VAWT sketch, and the “tunnel” that consists of the ODGV. Figure 3.7 show the mesh for the airfoil whereas figure 3.8 shows the meshes of the tunnel.

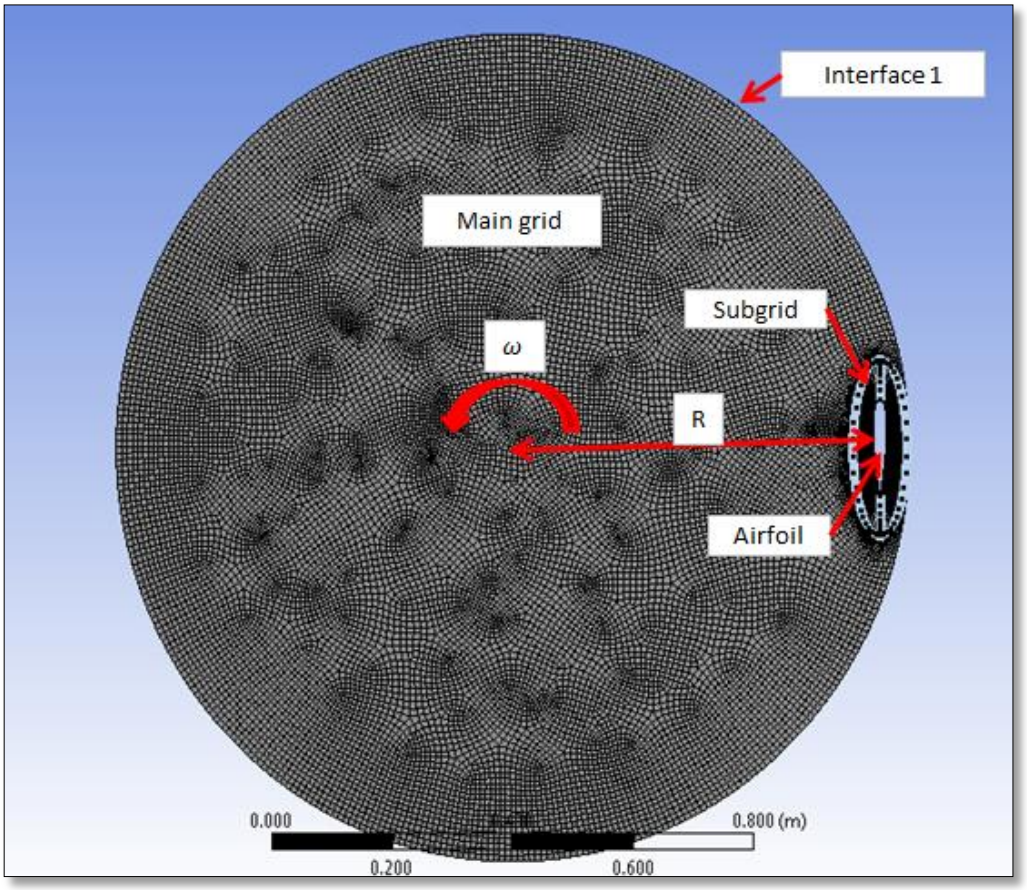

Figure 3.7: Airfoil mesh

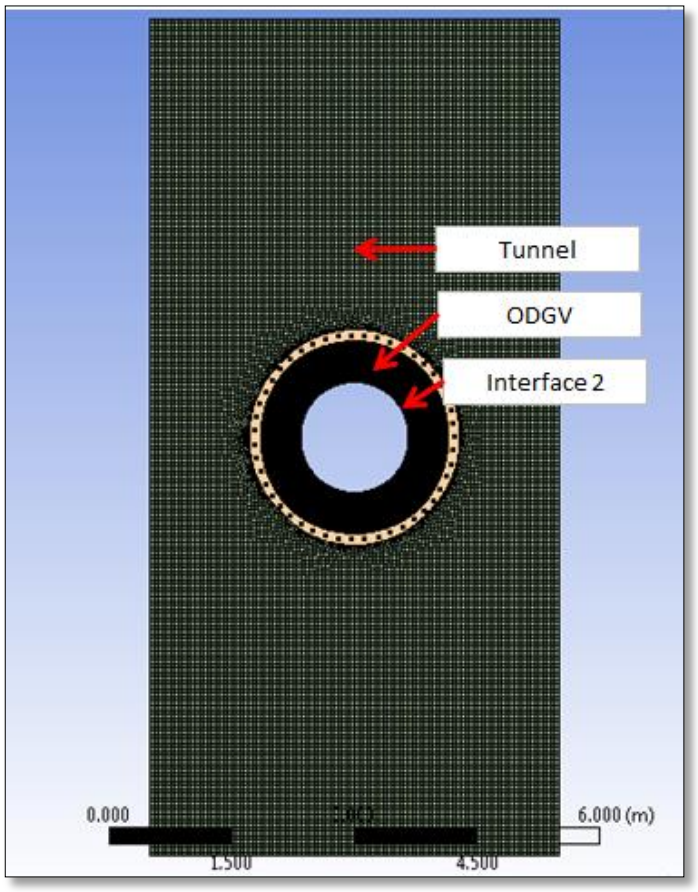

Figure 3.8: Tunnel mesh

The properties of the meshes are tabulated as following:

Table 3.2: Mesh sizing and method

Mesh	Region	Sizing (m)	Method	Total Nodes	Total elements
Airfoil	Main grid	0.01	Face sizing	322833	32355
	Sub grid	0.001	Face sizing, Mapped face meshing		
Tunnel	ODGV space	0.01	Face sizing	75256	73261
	Tunnel space	0.05	Face sizing		
	ODGV wall	0.003	Edge sizing		

Great attention is placed on the mesh at the area close to the blade profile (M. R. B. Castelli, S.D.; Benini E., 2012). In figure 3.9 shows the meshes for the leading edge of the NACA 0015 airfoil. From this figure, in order to create more consistent and organized mesh for the sub grid, the mapped face meshing function is used. Besides, the

sub grid of the airfoil mesh is divided into 2 regions by 2 partition lines. For this partition lines, it is using edge sizing by number of division of 30, with hard behaviour to create bias increasing element size. The bias factor used for these two partition line is 150. As can be seen from this figure, the computational meshes were constructed from lower topologies to higher along the airfoil profile. This edge sizing is important to make sure that the meshes near the airfoil wall are fine enough to get a promising simulation result by improve the CFD code capability in determining the flow separation, lift and drag of the blade (M. R. B. Castelli, S.D.; Benini E., 2012).

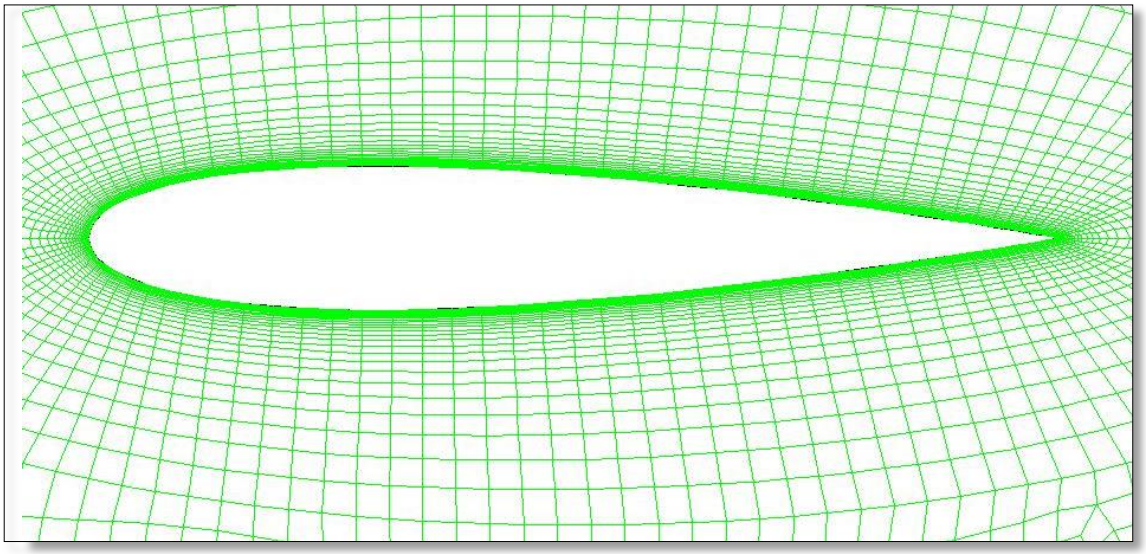

Figure 3.9: Near wall mesh of the NACA 0015

For good simulation practice, in order to obtain faster convergence, the mesh characteristic at both side of the interface need to be approximately same(M. R. S. Castelli, G. ; Benini,E. , 2012). Therefore, both of the main grid and the ODGV space is using the same cell size of 0.01m, face sizing. The tunnel space use the face sizing with 0.05m, this is because a larger size will be able to save time due to less nodes and element, hence less computational time. Whereas for the ODGV wall, the edge sizing of 0.003m is chosen, this is because the guide vanes thickness is 0.003m.This sizing can

obtain good discretization as shown in figure 3.10 and 3.11. Figure 3.12 shows the mesh after append both airfoil space mesh and tunnel space mesh.

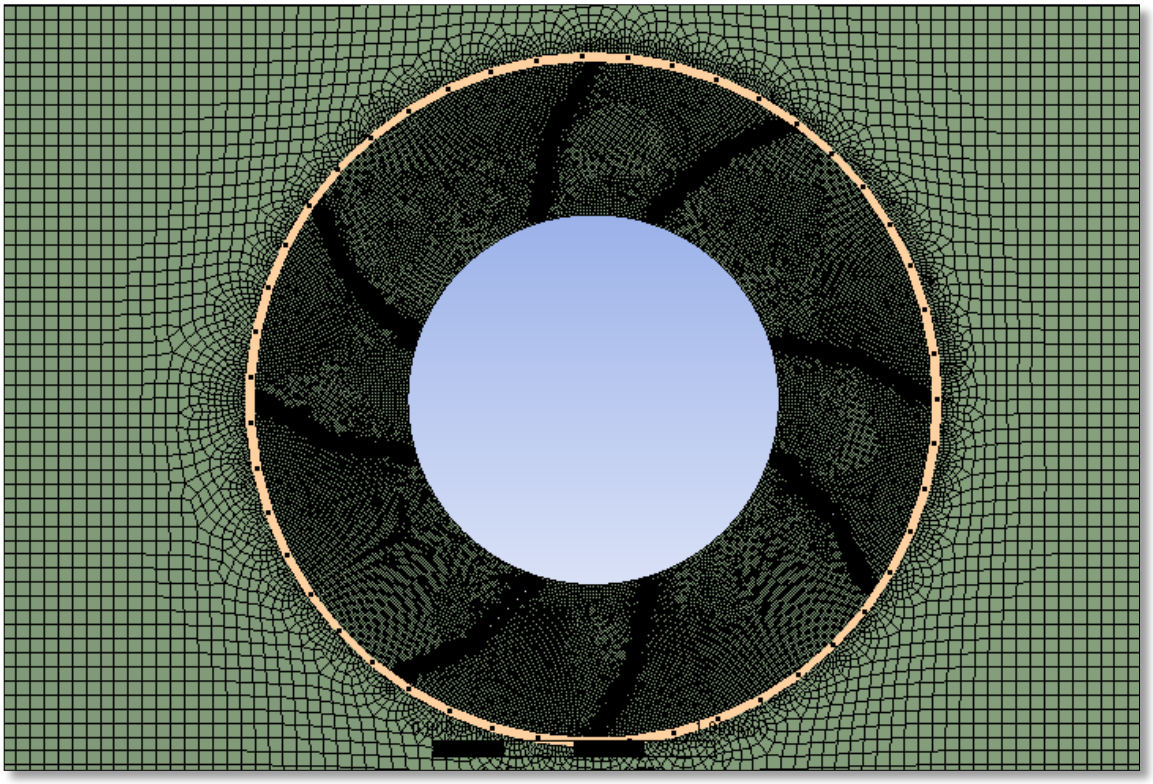

Figure 3.10: New ODGV mesh

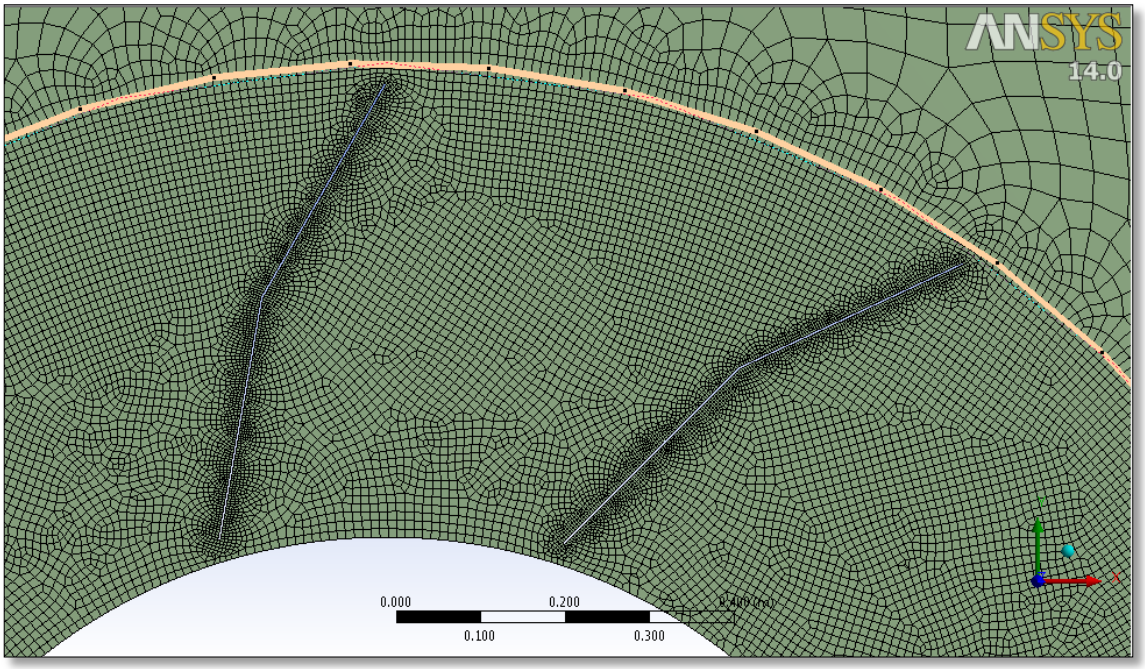

Figure 3.11: Near wall mesh for new ODGV

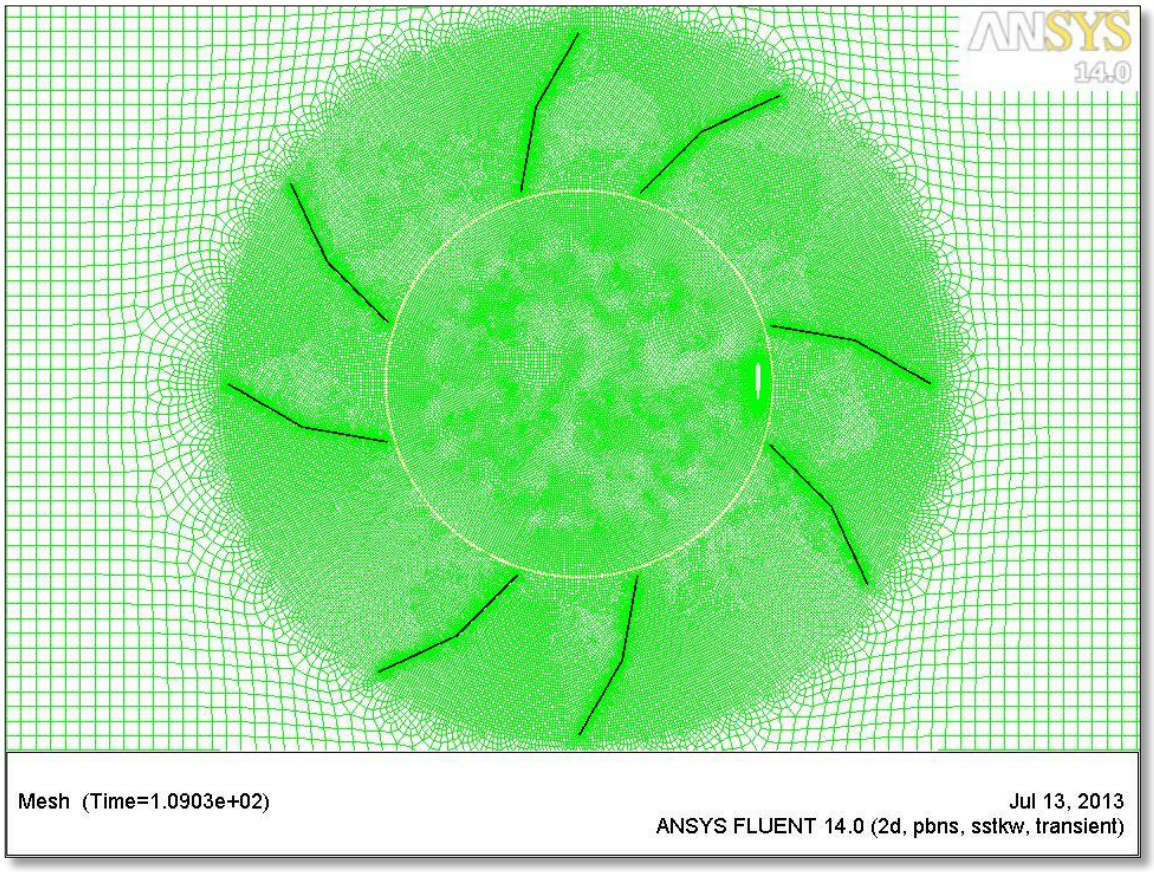

Figure 3.12: Mesh for airfoil space and tunnel space

3.5 Simulation setting

The simulation is repeated with the same boundary condition with Chong et al. simulation as summarize in the table 3.3. Figure 3.12 show the boundary conditions and the dimension of the simulation (Chong et al., 2013a). From this figure, the red line is the boundary for velocity inlet, and the yellow line indicates the pressure outlet. The dimension of the boundaries is followed Oler's experiment size, where the green lines are defined as wall. The airfoil space is located at the center of the tunnel, where the circumference around the VAWT rotational axis is set as interface to ensure the continuity of the flow field during the sliding mesh function (M. R. S. Castelli, G. ; Benini,E. , 2012).

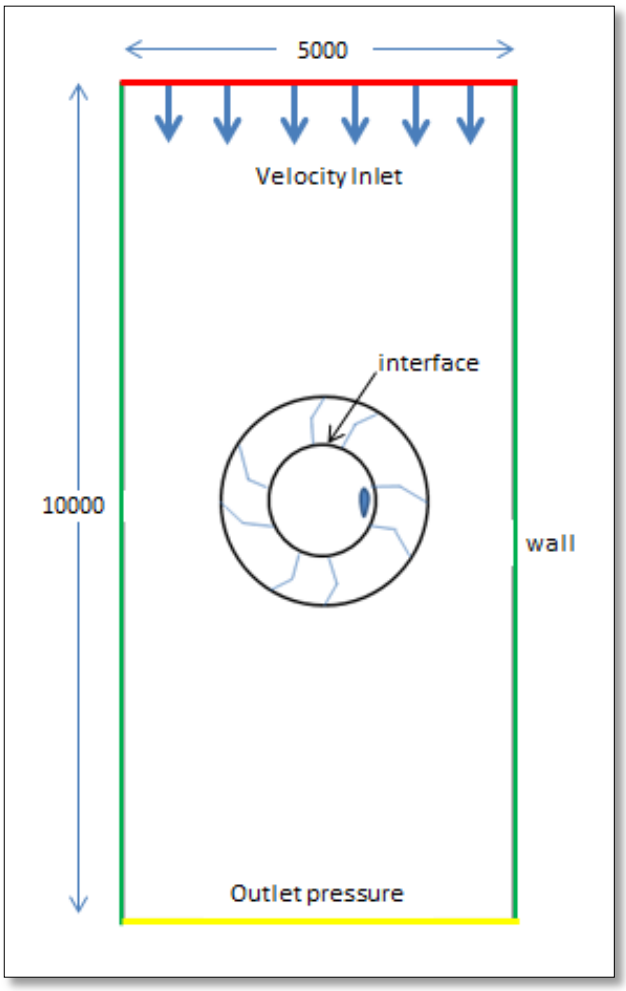

Figure 3.13: Boundary condition

Table 3.3: Computational conditions

Computational conditions	
Type	Pressure-Based
Time	Transient
Velocity formulation	Absolute
2D space	Planar
Viscous Model	k-ω model (SST)
Material	Water
Density	998.2 kg/m3
Viscosity	1.003 x 10-3 kg/m.s
Pressure	101,325 Pa
Blade Motion Type	Moving Mesh(Rotational)
Reference Frame	Absolute
Inlet Boundary Type	Velocity Inlet
Velocity inlet	0.091 m/s
Outlet Boundary Type	Pressure Outlet
Residual error	1 x 10-4
Pressure-velocity Coupling	SIMPLE scheme
Gradient	Green-Gauss Cell Based
Interpolating Scheme (Momentum)	2nd Order Upwind
Interpolating Scheme (Turbulence Kinetic Energy)	2nd Order Upwind
Interpolating Scheme (Specific Dissipation Rate)	2nd Order Upwind
Transient Formulation	2nd Order Implicit

3.6 k-ω SST Turbulence model

The turbulence model will influence the accuracy and the result of the simulation greatly. Among various RANS model, SST k-ω model by Menter *et al.*(2003) which blend the k-ω model for the near wall region and k-ε model for the far field region is considered a promising approach for simulation. It is well adapted for strong adverse pressure gradient flow and flow reversal that involve in the VAWT simulation (Li et al., 2013; Maître et al., 2013). Therefore, this k-ω SST model turbulence model is used to run the simulation.

The SST *k- ω* model is also known to have reduced sensitivity to far field values of turbulence frequency, *ω*, and a more balanced performance for a wide range of flow

types compared to other general-purpose two equation models (Chong et al., 2013a; Maître et al., 2013). The SST model is a variant from standard k-ω model where it combine the original Wilcox k-ω model which use for near wall region with the k-ε model for the far field and the eddy viscosity formulation to account for the transport of the principle shear stress. This model avoids the problem of too much k-ω sensitivity to the inlet free stream turbulence properties by switching to k-ε behavior. This turbulence model is quite popular for the VAWT simulation include Maître et al (2013), and Castelli et al. (2012)

3.7 Sliding mesh

The sliding mesh method is chosen rather than the rotating reference frame, this is because, after preliminary study, the former one gave more accurate result compare to the latter (Chong et al., 2013a). The sliding nesh method take the transient effect of the blade movement into account, whereas, the rotating reference frame is suitable for the flow situation where the stationary and the moving parts have no interaction, and in an instant time, the effect of rotation is calculated only("ANSYS FLUENT 12.0, Theory Guide," 2009). In the case of wind turbine simulation, where the transient rotor-stator interaction is desired, the sliding meshes method need to be used.

There are a few criteria need to be fulfilled in the mesh before using sliding mesh method as following ("ANSYS FLUENT 12.0, Tutorial Guide," 2009):

i) For sliding in a different relative speed, different cell zone need to be created.

ii) The motion for the sliding mesh must not be normal to the interface

iii) The shape of the interface can be any provided the interface boundaries are same geometry

iv) The periodic angle of the must be same for both rotor and stator

v) All periodic zones must be oriented correctly

Some other simulations conduct by Maître et al. (2013), Beri et al. (2011) and Pope et al. (2010) also performed CFD simulation of VAWT in sliding mesh method.

3.8 Enhanced wall treatment

In ANSYS FLUENT both $k-\omega$ models are available for the low-Reynold-number models and high-Reynold-number model. The mesh guidance should be same with the enhanced wall treatment. However, if the Low-Re Corrections option is enabled during the setting of the simulation in the Viscous Model, which purpose is to resolve the laminar sub-layer. In this case, the laminar sub-layer is adjacent to wall cells, then; the y^+ value should be in the range of 1 ("ANSYS FLUENT 12.0, User's Guide," 2009). According to Li et al.(2013), the mesh topologies can minimize the skewness of the near wall mesh and under high order of discretization, it can be fast converge. In order to resolve the laminar sub layer directly, the first mesh spacing on the airfoil profile set to be small enough to make the y+ value less than 1 (Li et al., 2013).

3.9 Pressure-velocity Coupling Scheme

The SIMPLE (Semi-Implicit Method for Pressure Linked Equations) algorithm of Patankar and Spalding (1972) was used to solve the conservation equations resulting from the discretization. The SIMPLE algorithm links both the mass conservation equation and momentum equations via pressure correction. SIMPLE is used in this study due to its computational efficiency, robustness in iterating the coupled parameters and higher-order differencing schemes. The convective terms were numerically differentiated with the linear upwind differencing scheme, providing a balance between accuracy and computing cost. Similar to Mohamed (2012) simulation, the pressure velocity coupling is solved by using SIMPLE algorithm for the Unsteady Reynolds-

Averaged Navier-Stokes equation. The discretization is using FVM with second order upwind scheme for all variables (Mohamed, 2012).

3.10 Coefficient of Torque

There is a function in ANSYS FLUENT for the user to monitor the coefficient of torque which created on by the airfoil blade. It will capture difference of the surface pressure on the NACA 0015 airfoil blade, and calculate the force hence the torque. This coefficient of torque, Ct is in a non-dimensional form. The data capture for every 10 degree until the iteration is converge to the convergence limit that set. After the simulation is stable, a set of date was being average as $Ct_{avg.}$ The average power for the VAWT is calculated as following:

$$Ct = \frac{\tau}{\frac{1}{2}.\rho.c.H.Vin^2.R} \quad (3.1)$$

$$Cp\ avg = Ct\ avg.TSR.\frac{c}{2R} \quad (3.2)$$

\\

CHAPTER 4 RESULTS AND DISCUSSION

4.1 Validation of Simulation Result

The simulation is verified with the Oler's experiment published by the Sandia National Laboratories. The torque coefficient that capture from the simulation versus azimuth angle is plotted and compared to the experiment data at TSR 5.1. From the simulation results, it demonstrates a good agreement curve pattern with the experiment date. Figure 4.1 show the torque coefficient versus azimuth angle, from this graph, it show that the peak value of the torque coefficient at approximate 120^{o} is over estimated. Deglaire et al. (2009) explained that this over estimation is because of low Reynolds number consideration which increase the drag and significant decreases the lift of the blade. Therefore the upwind power extracted is too high and the downwind speed is reduced too much hence simulated low normal forces (Chong et al., 2013a; Deglaire, Engblom, Ågren, & Bernhoff, 2009). Besides, according to Roy et al. show that although the shear stress transport (SST) k-ω turbulence model has a general agreement with the actual experiment result, the 2D simulation result show over predicted compare to experiment data, whereas for 3D simulation will obtain a better result (Roy & Saha, 2013). The coefficient of torque versus flow time for 10 cycles is shown in Appendix C

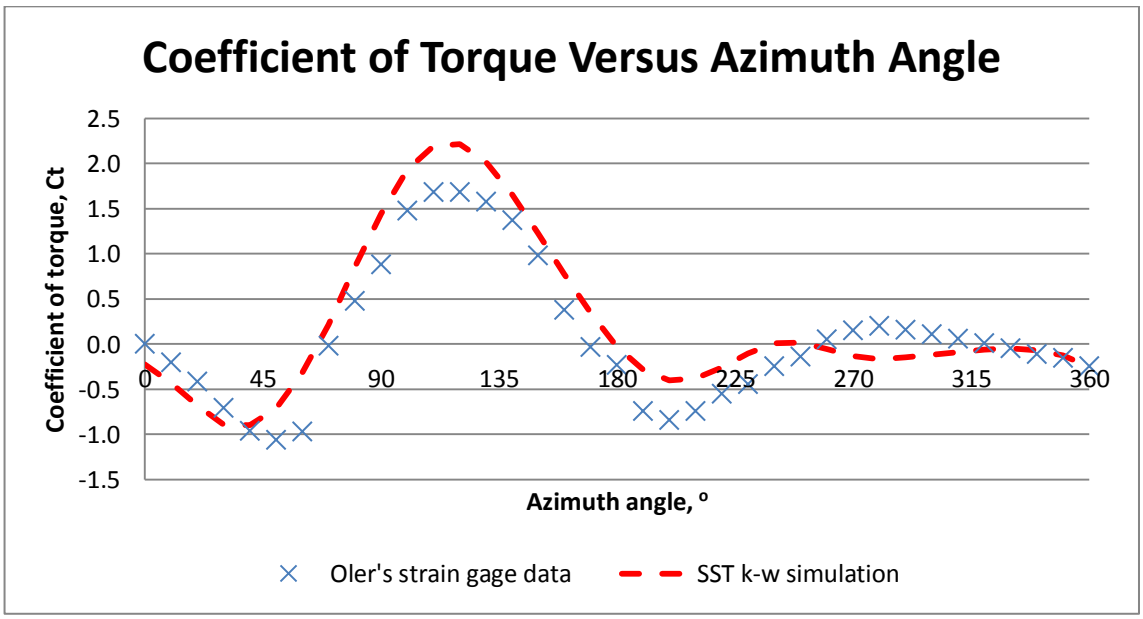

Figure 4.1: Coefficient of torque versus azimuth angle for bare VAWT

The y+ value for the airfoil blade is observed, and the result show that with the meshing method with the topologies from lower near the airfoil profile to the higher one is able to performed a good transient flow. Figure 4.2 show that most of the points near the airfoil blade fall below value 1 for the y+ value. Figure 4.3 and 4.4 show the velocity contour for the original ODGV simulation.

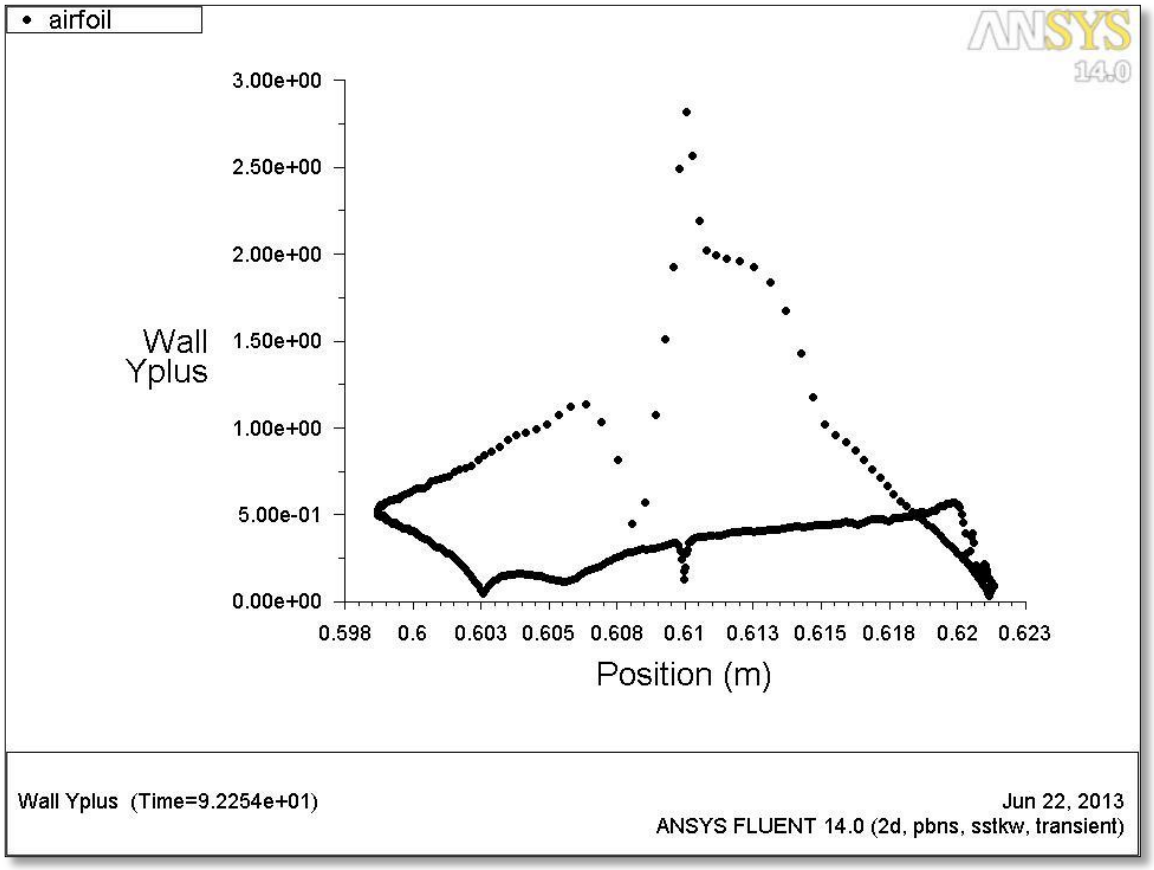

Figure 4.2: y+ value for the bare VAWT

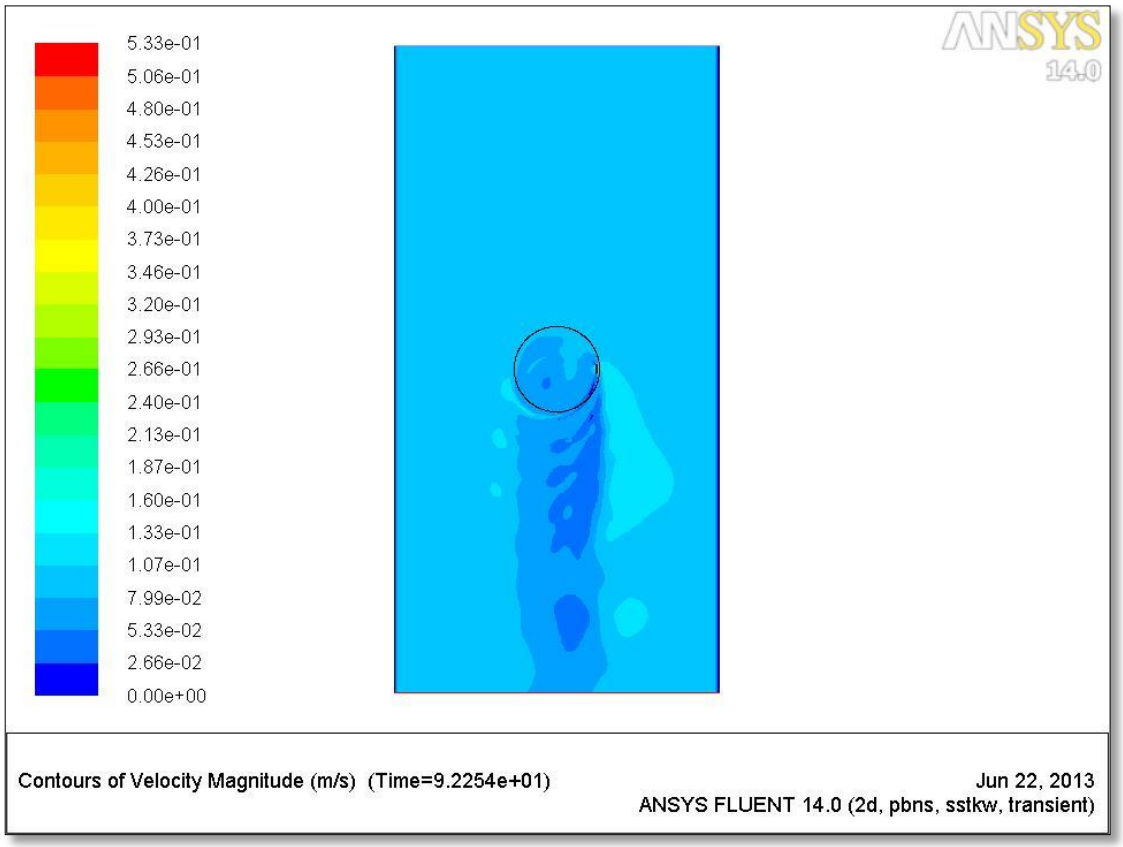

Figure 4.3: Velocity contour for bare VAWT

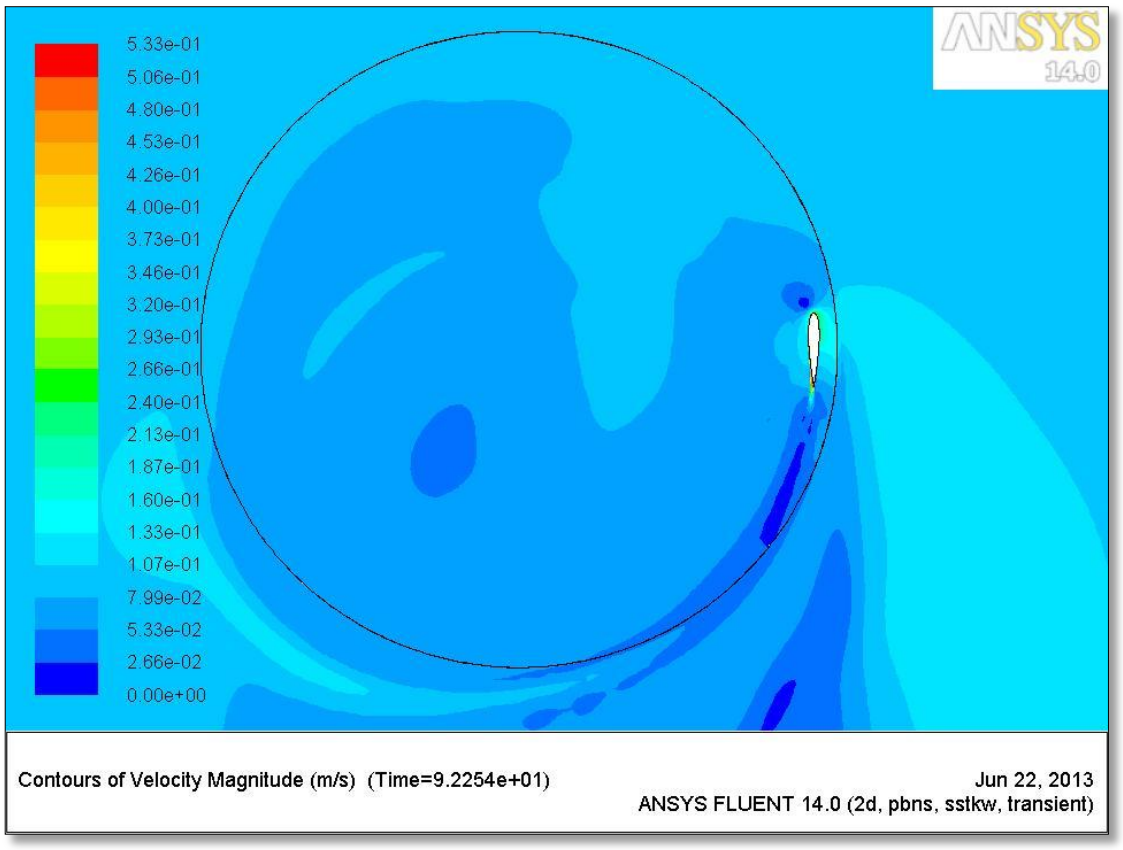

Figure 4.4: Detail view of velocity contour for bare VAWT

4.2 Omni-directional Guide Vane Simulation

When compare with Chong et al. simulation on the ODGV integrated with VAWT (Chong et al., 2013a) . The simulation result also show similar curve pattern. The average torque coefficient from Chong et al. simulation with the presence of original ODGV is 0.4195, whereas for the re-simulate result, the average torque obtained is 0.4052. This variance is due to the modelling of the domain and meshing method is slightly different. Figure 4.5 show the simulation result for the VAWT and the VAWT with original ODGV. The coefficient of torque versus flow time for 10 cycles is shown in Appendix C. Most of the point of the airfoil blade wall having the y+ value less than 1 as shown in figure 4.6. Figure 4.7 and 4.8 show the velocity contour for the original ODGV simulation.

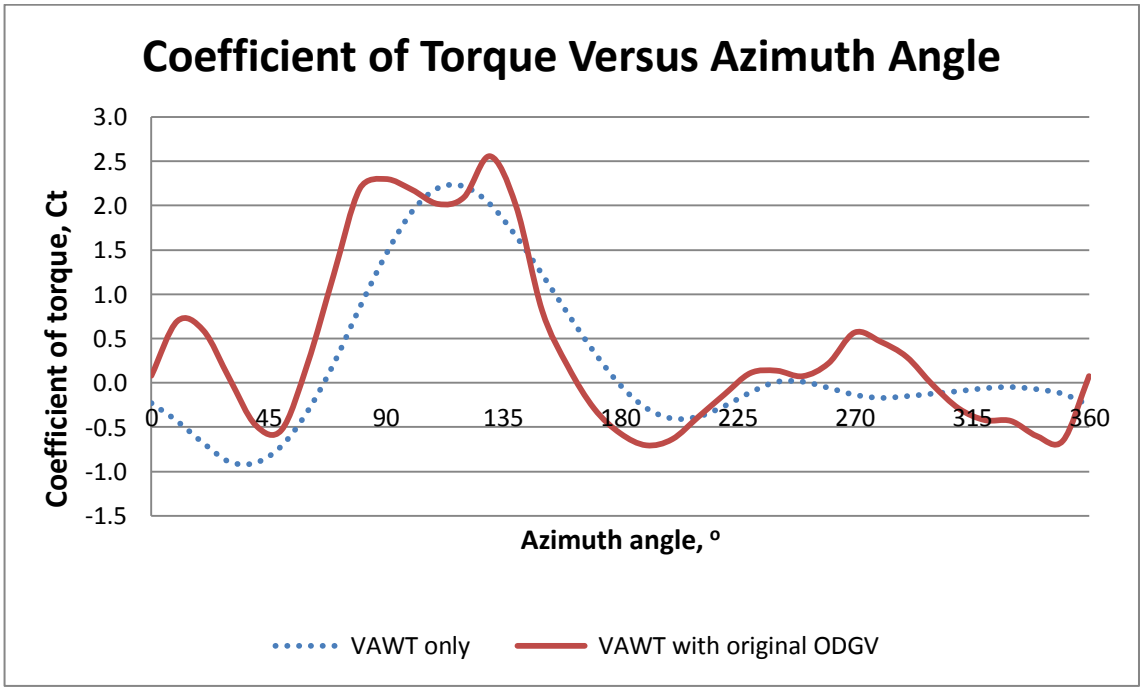

Figure 4.5: Coefficient of torque versus azimuth angle for bare VAWT and VAWT with original ODGV

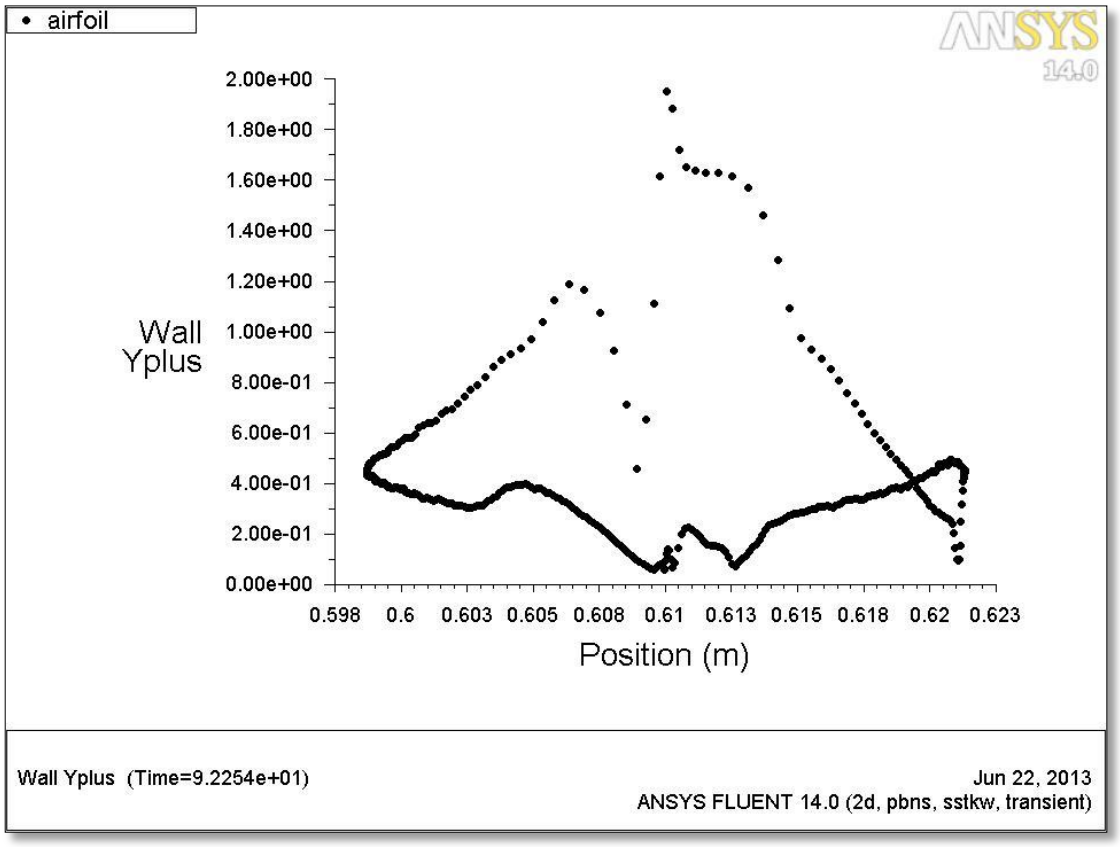

Figure 4.6: y+ value for the VAWT with original ODGV

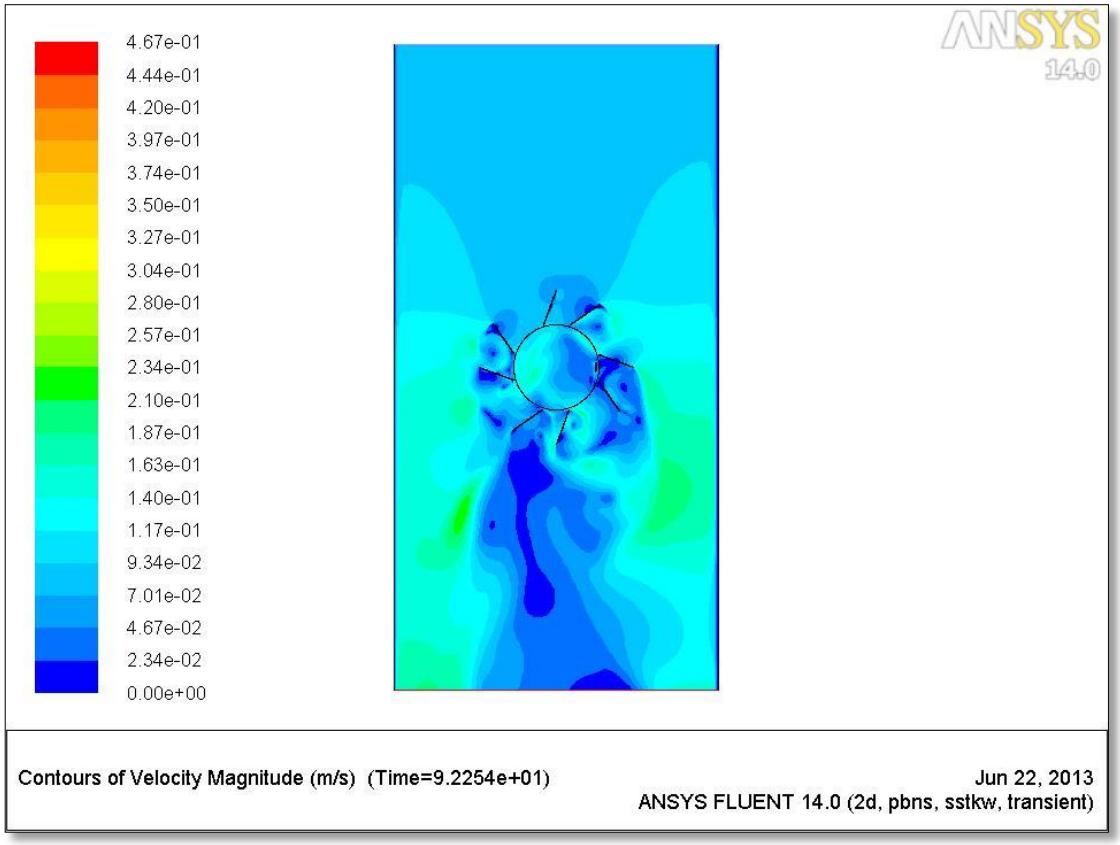

Figure 4.7: Velocity contour for VAWT with original ODGV

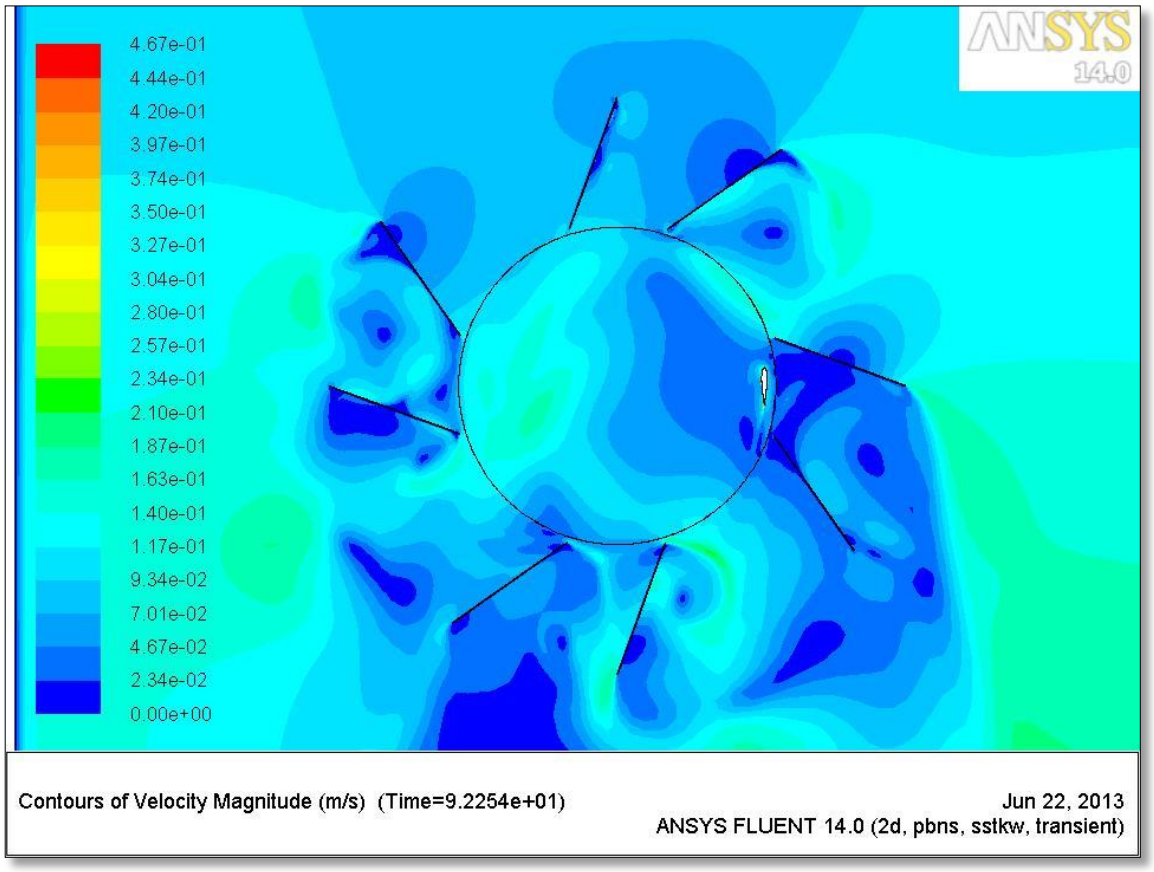

Figure 4.8: Detail view for velocity contour for VAWT with original ODGV

4.3 New Omni-directional Guide Vane Design Simulation

The coefficient of torque for new ODGV design and the original ODGV is plotted in Figure 4.9. The graph shows that both of the ODGV designs have the similar curve trend, the new ODGV design is slightly improve the Ct before azimuth angle approximate 180^{o}. From azimuth angle 180^{o} to 270^{o}, it shows significant increase of the Ct. The average torque for the new ODGV design is 0.5333, which is about 31.6 % increased compare to the original design. The coefficient of torque versus flow time for 10 cycles is shown in Appendix C. The y+ value is less than 1 as shown in figure 4.10. Figure 4.11 and 4.12 show the velocity contour for the original ODGV simulation.

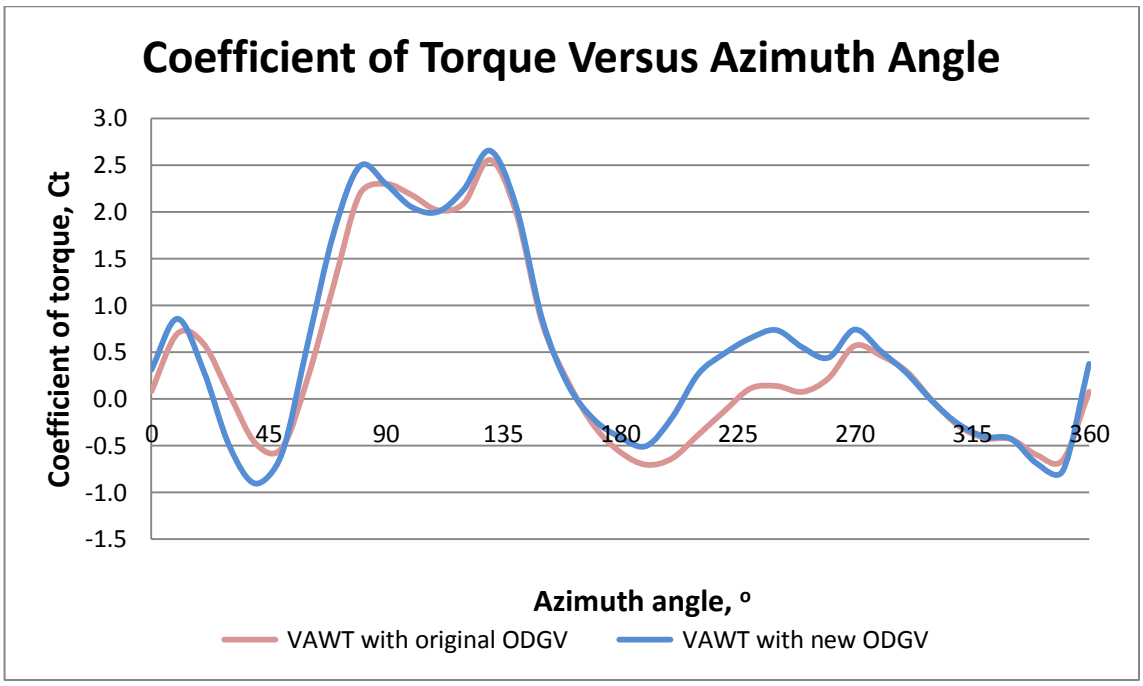

Figure 4.9: Coefficient of torque versus azimuth angle for VAWT with original ODGV and new ODGV

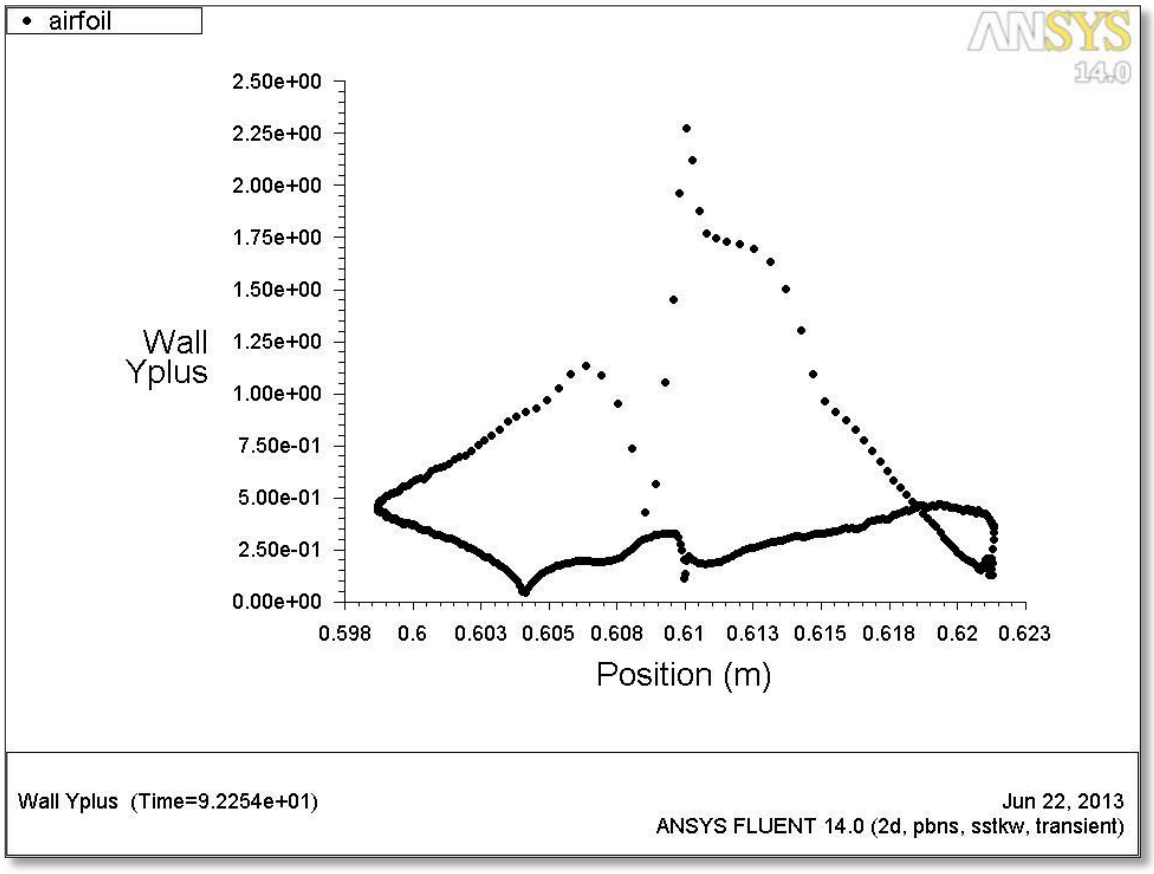

Figure 4.10: y+ value for the VAWT with new ODGV

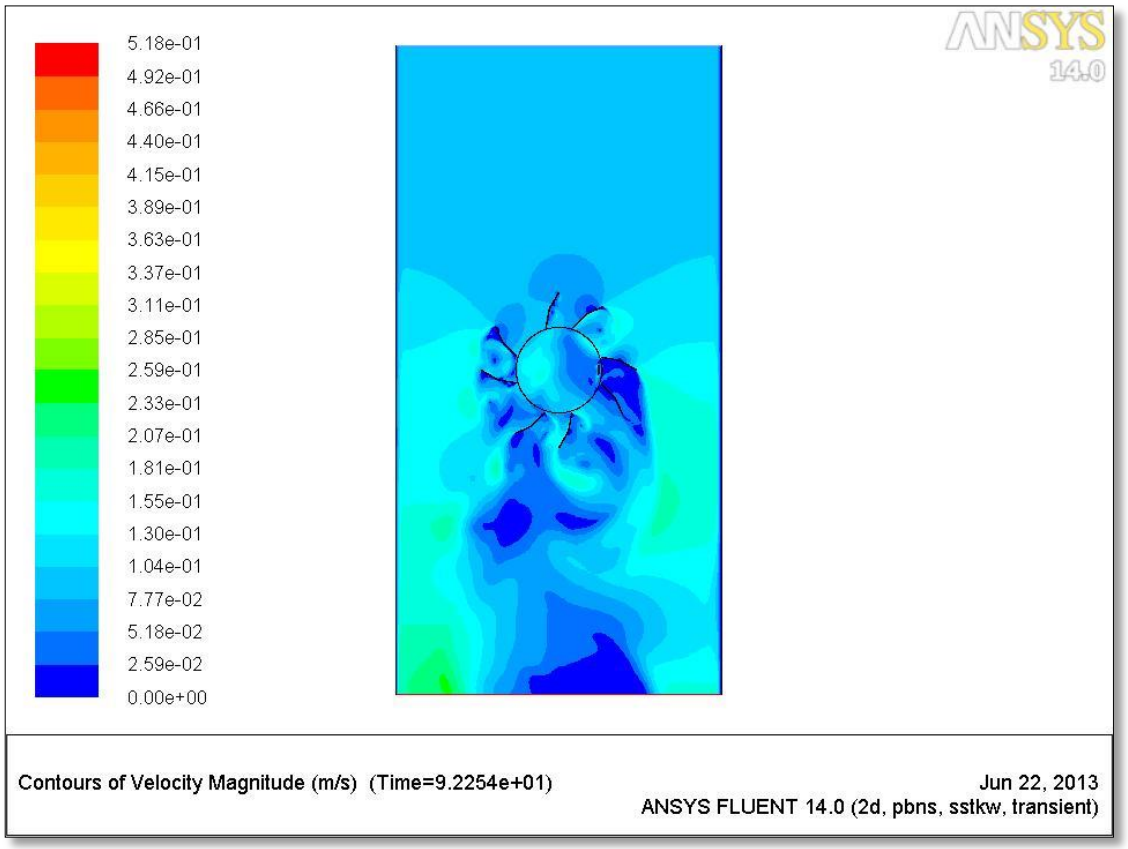

Figure 4.11: Velocity contour for VAWT with new ODGV

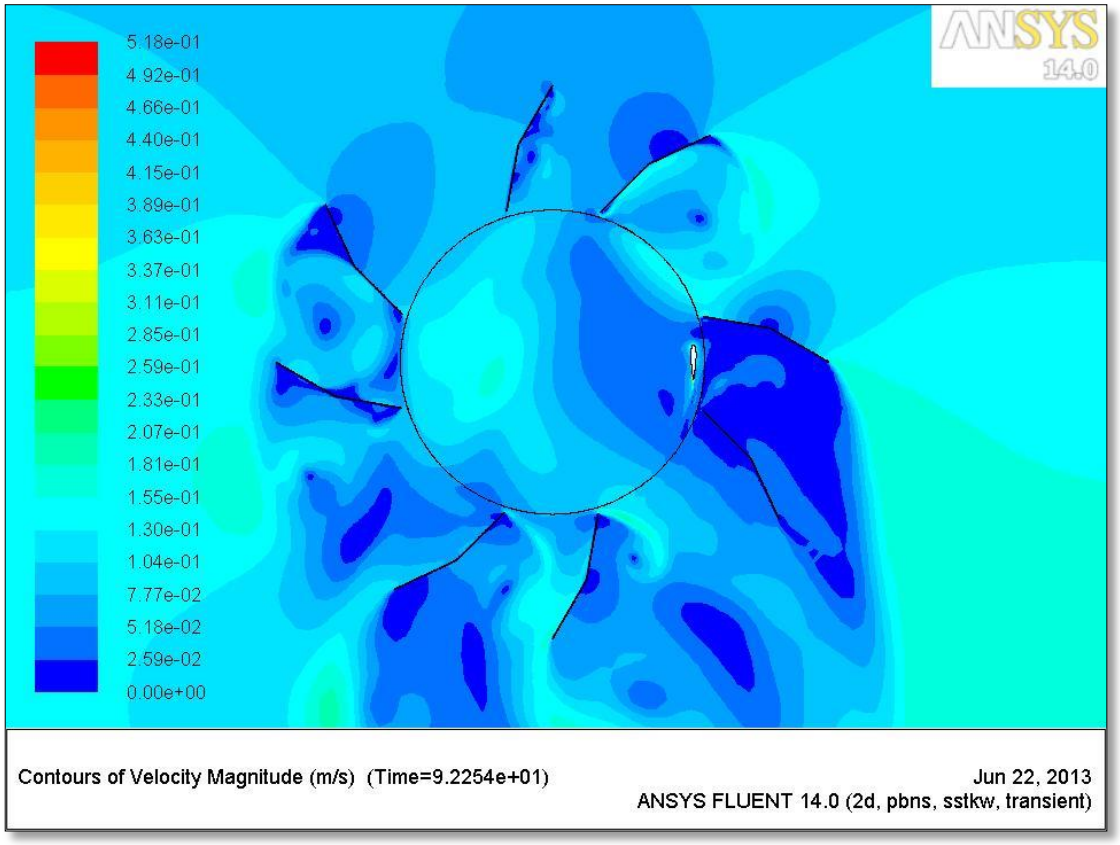

Figure 4.12: Detail view for velocity contour for VAWT with new ODGV

The result for the simulation is summarized in table 4.1 below by calculated using equation 3.2. From this table, it show that the ODGV can significant improve the performance of VAWT, moreover, the new ODGV design can further increase the Coefficient of Power from 0.2581 to 0.3398 which in percentage by 31.65%. If compare to the bare VAWT, it is about 115.56 %, which is almost twice of the power coefficient.

The coefficient of power, Cp for a wind turbine is the efficiency of the wind turbine converts the kinetic energy from the wind to electrical energy. It is also the ratio of the power generated to the total power of the wind at certain wind speed.

$$\text{Coefficient of power, Cp} = \frac{\text{Power generated by wind turbine}}{\text{Total power from the wind}}$$

Table 4.1: Comparison of coefficient of torque and coefficient of power

	VAWT	with original ODGV	with new ODGV
Average Coefficien of Torque, Ct,avg	0.2158	0.4052	0.5333
Coefficient of Power, Cp	0.1375	0.2581	0.3398

CHAPTER 5 CONCLUSION

The major idea for the present work is to improve the performance of the VAWT by the design of power augmented shroud. A new power augmented shroud which is modified from Chong et al. (2013a) ODGV was designed and analysed by numerical method. This new design remains four pairs of guide vane at the azimuth angle of $0^{o,}$ 90^{o}, 180^{o} and 360^{o}. Each pairs of the blade with an angle of 20^{o} and 55^{o} degree normal to the axis of the VAWT rotor. The new design divides the original guide vane into two pieces with a 10 degree angle tilted.

Numerical analysis was performed on the NACA 0015 airfoil in order to understand the effect of the ODGV on the output for the VAWT by using commercial CFD software ANSYS FLUENT 14.0. The k-ω SST turbulence model with the sliding mesh function was used in this simulation. The simulation is verified by the Oler's experiment date published by the Sandia National Laboratories.

From the simulation result, the ODGV integrated with VAWT is able to get a significant improve for the coefficient of power. The new design of the ODGV is further improve the original design by 31.65%. This performance increase due to the optimization of the incoming wind speed, and channel the wind by the ODGV to make a better angle of attack to the VAWT blade, hence improve the self-starting torque for the VAWT.

As conclusion, from the simulation result, the new ODGV design integrated with VAWT is appropriate to be used in urban area where the wind speed is low and wind direction is inconsistent due to the shadow effect of the high rise building. The design can lower down the cut in speed, so that the VAWT has a lower self-starting torque, hence a long duration for the working hour.

REFERENCES

Abohela, I., Hamza, N., & Dudek, S. (2013). Effect of roof shape, wind direction, building height and urban configuration on the energy yield and positioning of roof mounted wind turbines. *Renewable Energy, 50*(0), 1106-1118. doi: http://dx.doi.org/10.1016/j.renene.2012.08.068

ANSYS FLUENT 12.0, Theory Guide. (2009).

ANSYS FLUENT 12.0, Tutorial Guide. (2009).

ANSYS FLUENT 12.0, User's Guide. (2009).

Aslam Bhutta, M. M., Hayat, N., Farooq, A. U., Ali, Z., Jamil, S. R., & Hussain, Z. (2012). Vertical axis wind turbine – A review of various configurations and design techniques. *Renewable and Sustainable Energy Reviews, 16*(4), 1926-1939. doi: http://dx.doi.org/10.1016/j.rser.2011.12.004

Asress, A. M. S., A.; Komarov,D.;Stupar,S. (2013). Numerical and Analytical Investigation of Vertical Axis Wind Turbine. *FME Transactions, 41*(1), 49-85.

Castelli, M. R. B., S.D.; Benini E. (2012). Effect of Blade Number on a Straight-Bladed Vertical-Axis Darrieus wind turbine. *World Academy of Science, Engineering and Technology, 61*.

Castelli, M. R. S., G. ; Benini,E. . (2012). Numerical Analysis of the Influence of Airfoil Asymmetry on VAWT Performance. *World Academy of Science, Engineering and Technology, 61*.

Chong, W. T., Fazlizan, A., Poh, S. C., Pan, K. C., Hew, W. P., & Hsiao, F. B. (2013a). The design, simulation and testing of an urban vertical axis wind turbine with the omni-direction-guide-vane. *Applied Energy*(0). doi: http://dx.doi.org/10.1016/j.apenergy.2012.12.064

Chong, W. T., Fazlizan, A., Poh, S. C., Pan, K. C., & Ping, H. W. (2012). Early development of an innovative building integrated wind, solar and rain water harvester for urban high rise application. *Energy and Buildings, 47*(0), 201-207. doi: http://dx.doi.org/10.1016/j.enbuild.2011.11.041

Chong, W. T., Naghavi, M. S., Poh, S. C., Mahlia, T. M. I., & Pan, K. C. (2011). Techno-economic analysis of a wind–solar hybrid renewable energy system with rainwater collection feature for urban high-rise application. *Applied Energy, 88*(11), 4067-4077. doi: http://dx.doi.org/10.1016/j.apenergy.2011.04.042

Chong, W. T., Pan, K. C., Poh, S. C., Fazlizan, A., Oon, C. S., Badarudin, A., & Nik-Ghazali, N. (2013b). Performance investigation of a power augmented vertical axis wind turbine for urban high-rise application. *Renewable Energy, 51*(0), 388-397. doi: http://dx.doi.org/10.1016/j.renene.2012.09.033

Deglaire, P., Engblom, S., Ågren, O., & Bernhoff, H. (2009). Analytical solutions for a single blade in vertical axis turbine motion in two-dimensions. *European*

Journal of Mechanics - B/Fluids, 28(4), 506-520. doi: http://dx.doi.org/10.1016/j.euromechflu.2008.11.004

Eriksson, S., Bernhoff, H., & Leijon, M. (2008). Evaluation of different turbine concepts for wind power. *Renewable and Sustainable Energy Reviews, 12*(5), 1419-1434. doi: http://dx.doi.org/10.1016/j.rser.2006.05.017

Islam, M., Ting, D. S. K., & Fartaj, A. (2008). Aerodynamic models for Darrieus-type straight-bladed vertical axis wind turbines. *Renewable and Sustainable Energy Reviews, 12*(4), 1087-1109. doi: http://dx.doi.org/10.1016/j.rser.2006.10.023

Islam, M. R., Mekhilef, S., & Saidur, R. (2013). Progress and recent trends of wind energy technology. *Renewable and Sustainable Energy Reviews, 21*(0), 456-468. doi: http://dx.doi.org/10.1016/j.rser.2013.01.007

Kim, D., & Gharib, M. (2013). Efficiency improvement of straight-bladed vertical-axis wind turbines with an upstream deflector. *Journal of Wind Engineering and Industrial Aerodynamics, 115*(0), 48-52. doi: http://dx.doi.org/10.1016/j.jweia.2013.01.009

Ledo, L., Kosasih, P. B., & Cooper, P. (2011). Roof mounting site analysis for micro-wind turbines. *Renewable Energy, 36*(5), 1379-1391. doi: http://dx.doi.org/10.1016/j.renene.2010.10.030

Li, C., Zhu, S., Xu, Y.-l., & Xiao, Y. (2013). 2.5D large eddy simulation of vertical axis wind turbine in consideration of high angle of attack flow. *Renewable Energy, 51*(0), 317-330. doi: http://dx.doi.org/10.1016/j.renene.2012.09.011

Maître, T., Amet, E., & Pellone, C. (2013). Modeling of the flow in a Darrieus water turbine: Wall grid refinement analysis and comparison with experiments. *Renewable Energy, 51*(0), 497-512. doi: http://dx.doi.org/10.1016/j.renene.2012.09.030

McTavish, S., Feszty, D., & Sankar, T. (2012). Steady and rotating computational fluid dynamics simulations of a novel vertical axis wind turbine for small-scale power generation. *Renewable Energy, 41*(0), 171-179. doi: http://dx.doi.org/10.1016/j.renene.2011.10.018

Mohamed, M. H. (2012). Performance investigation of H-rotor Darrieus turbine with new airfoil shapes. *Energy, 47*(1), 522-530. doi: http://dx.doi.org/10.1016/j.energy.2012.08.044

Müller, G., Jentsch, M. F., & Stoddart, E. (2009). Vertical axis resistance type wind turbines for use in buildings. *Renewable Energy, 34*(5), 1407-1412. doi: http://dx.doi.org/10.1016/j.renene.2008.10.008

Nobile, R. V., M.; Barlow,J.; Mewburn-Crook,A. (2011). Dynamic Stall for a Vertical Axis Wind Turbine in a Two-dimensional Study. *World Renewable Energy Congress, 8-13 May 2011*.

Oler, J. W. S., J.H.; Graham,B.J.Im,G.H. (1983). Dynamic Stall Regulation of the Darriues Turbine. *Sandia National Laboratories (SAND 83-7029 UC-261), Albuquweque, New Mexico*.

Pope, K., Rodrigues, V., Doyle, R., Tsopelas, A., Gravelsins, R., Naterer, G. F., & Tsang, E. (2010). Effects of stator vanes on power coefficients of a zephyr vertical axis wind turbine. *Renewable Energy, 35*(5), 1043-1051. doi: http://dx.doi.org/10.1016/j.renene.2009.10.012

Roy, S., & Saha, U. K. (2013). Review on the numerical investigations into the design and development of Savonius wind rotors. *Renewable and Sustainable Energy Reviews, 24*(0), 73-83. doi: http://dx.doi.org/10.1016/j.rser.2013.03.060

Sharpe, T., & Proven, G. (2010). Crossflex: Concept and early development of a true building integrated wind turbine. *Energy and Buildings, 42*(12), 2365-2375. doi: http://dx.doi.org/10.1016/j.enbuild.2010.07.032

Toja-Silva, F., Colmenar-Santos, A., & Castro-Gil, M. (2013). Urban wind energy exploitation systems: Behaviour under multidirectional flow conditions—Opportunities and challenges. *Renewable and Sustainable Energy Reviews, 24*(0), 364-378. doi: http://dx.doi.org/10.1016/j.rser.2013.03.052

Walker, S. L. (2011). Building mounted wind turbines and their suitability for the urban scale—A review of methods of estimating urban wind resource. *Energy and Buildings, 43*(8), 1852-1862. doi: http://dx.doi.org/10.1016/j.enbuild.2011.03.032

Wang, S., Ingham, D. B., Ma, L., Pourkashanian, M., & Tao, Z. (2010). Numerical investigations on dynamic stall of low Reynolds number flow around oscillating airfoils. *Computers & Fluids, 39*(9), 1529-1541. doi: http://dx.doi.org/10.1016/j.compfluid.2010.05.004

Yao, Y. X., Tang, Z. P., & Wang, X. W. (2013). Design based on a parametric analysis of a drag driven VAWT with a tower cowling. *Journal of Wind Engineering and Industrial Aerodynamics, 116*(0), 32-39. doi: http://dx.doi.org/10.1016/j.jweia.2012.11.001

Internet Reference:

Top 10 Major Environment Issues In The World Today. Retrieved October 9 2012, from http://www.safety-security-crazy.com/major-environmental-issues.html

Malaysia Explores Its Renewables Options. Retrieved October 15 2012, from http://www.renewableenergyworld.com/rea/news/article/2011/09/malaysia-explores-its-renewables-options

NACA 0015. Retrieved June 12 2013, from http://airfoiltools.com/airfoil/details?airfoil=naca0015-il

Bahrain World Trade Centre. Retrieved June 12 2013, from http://www.bahrainwtc.com/

Bolte Bridge. Retrieved June 12 2013, from http://multimedia.aapnewswire.com.au/Search.aspx?search=%22Wind+Turbine%22&field=ObjectName&Gallery=Wind+Turbine

Understanding Coefficient of Power (Cp) and Betz Limit, Retrieved August 13, from http://learn.kidwind.org/sites/default/files/betz_limit_0.pdf

APPENDIX

APPENDIX A:

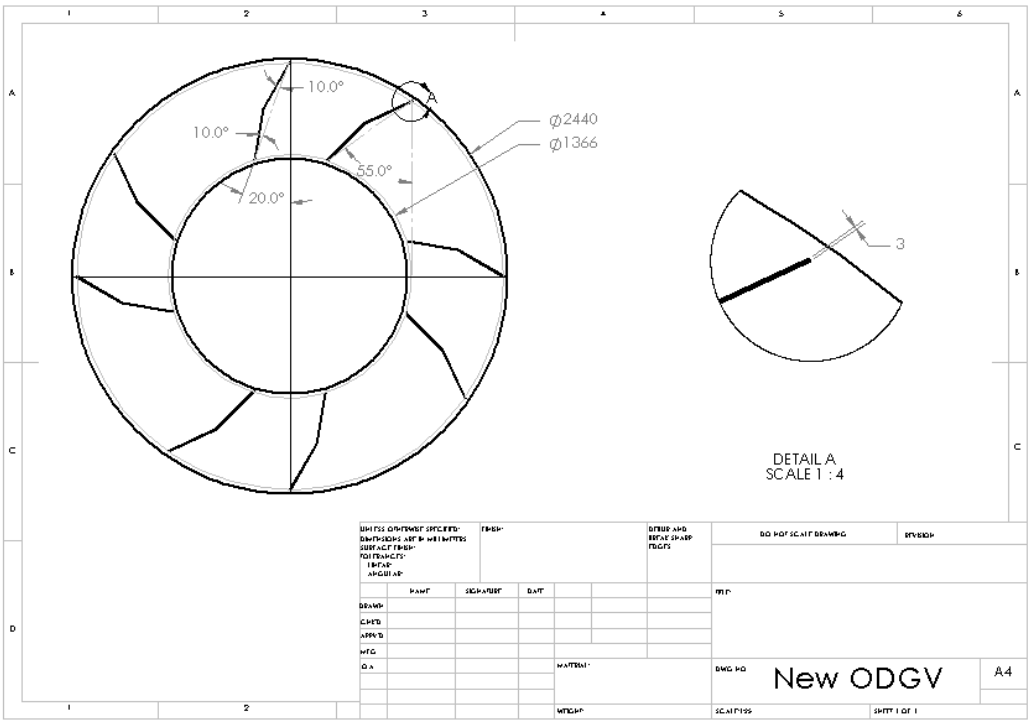

New ODGV drawing

APPENDIX B:

Coordinate for NACA 0015-airfoil

NACA 0015	
1.0000	0.00158
0.9500	0.01008
0.9000	0.01810
0.8000	0.03279
0.7000	0.04580
0.6000	0.05704
0.5000	0.06617
0.4000	0.07254
0.3000	0.07502
0.2500	0.07427
0.2000	0.07172
0.1500	0.06682
0.1000	0.05853
0.0750	0.05250
0.0500	0.04443
0.0250	0.03268
0.0125	0.02367
0.0000	0.00000
0.0125	-0.02367
0.0250	-0.03268
0.0500	-0.04443
0.0750	-0.05250
0.1000	-0.05853
0.1500	-0.06682
0.2000	-0.07172
0.2500	-0.07427
0.3000	-0.07502
0.4000	-0.07254
0.5000	-0.06617
0.6000	-0.05704
0.7000	-0.04580
0.8000	-0.03279
0.9000	-0.01810
0.9500	-0.01008
1.0000	-0.00158

APPENDIX C:

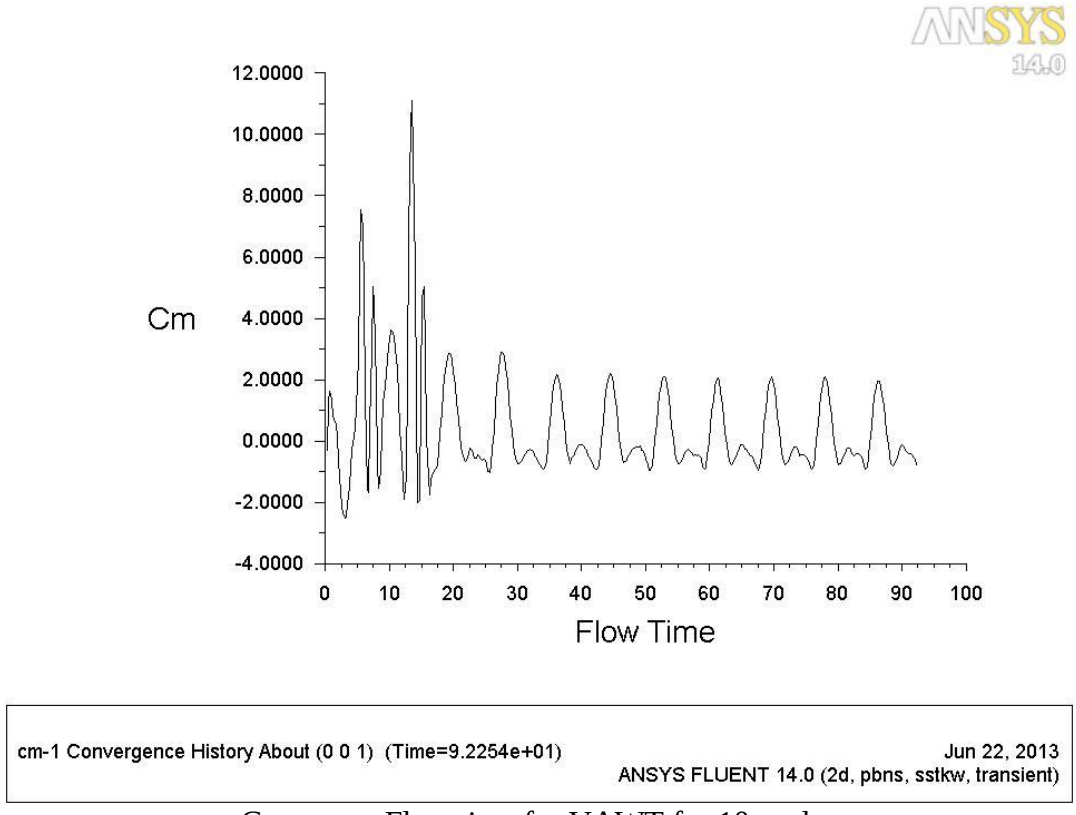

Cm versus Flow time for VAWT for 10 cycles

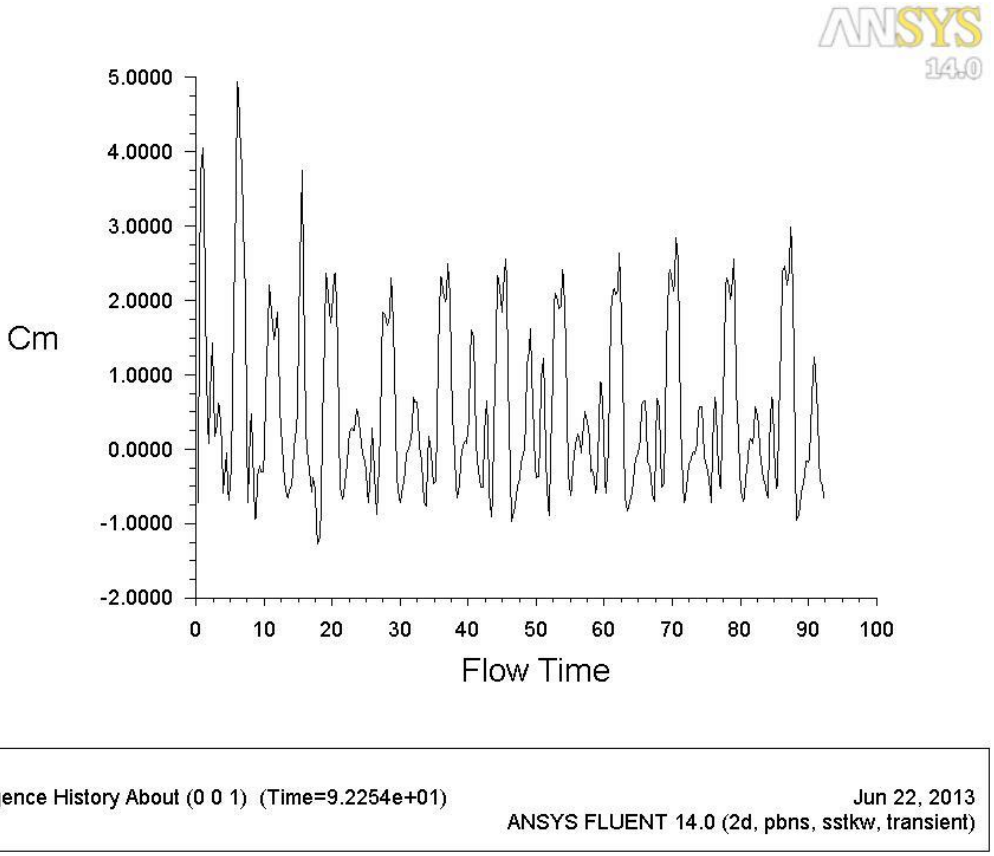

Cm versus Flow time for VAWT for 10 cycles

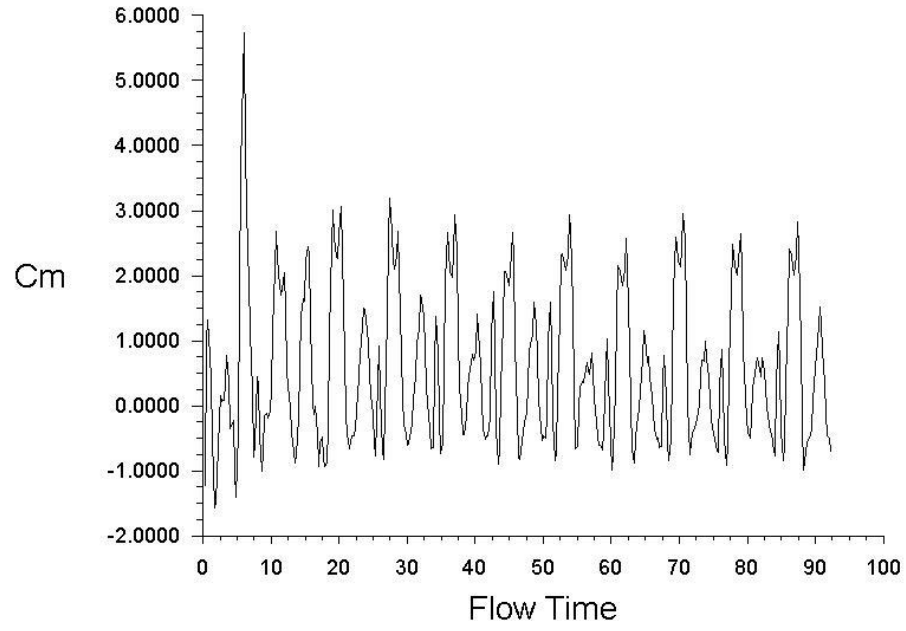

Cm versus Flow time for new ODGV design with VAWT for 10 cycles